Supercritical Fluid Nanospray Mass Spectrometry

II. Effects on Ionization

Mahmoud Elhusseiny Mostafa¹, Madisyn M. Hayes², James P. Grinias³, Benjamin J. Bythell², and James L. Edwards¹*

ABSTRACT: Nanospraying supercritical fluids coupled to a mass spectrometer (nSF-MS) using 90 % CO₂ carrier (sCO₂) has shown an enhanced desolvation compared to traditional liquid eluents. Capillaries with 25, 50, and 75 μm internal diameter (i.d.) with pulled emitter tips provided high MS detection sensitivity. Presented here is an evaluation of the effect of proton affinity, hydrophobicity, and nano emitter tip size on the nSF-MS signal. This was done using a set of primary, secondary, tertiary, and quaternary amines with butyl-, hexyl-, octyl-, and decyl- chains as analytes. Each amine class was analyzed individually to evaluate hydrophobicity and proton affinity effects on signal intensity. The system has shown a mass-sensitive detection on a linear dynamic range of 0.1 – 100 μM. Results indicate that hydrophobicity has a larger effect on the signal response than proton affinity. Nanospraying a mixture of all amine classes using the 75 μm emitter has shown a quaternary amine signal not suppressed by competing analytes. Competing ionization was observed for primary, secondary, and tertiary amines. The 75 and 50 μm emitters demonstrated increased signal with increasing hydrophobicity. Surprisingly, the 25 μm i.d. emitter yielded a signal decrease as the alkyl chain length increased, contrary to conventional understanding. Nanospraying the evaporative fluid in a sub 500 nm emitter likely resulted in differences in the ionization mechanism. Results suggest that 90 % sCO₂ with 9.99 % methanol and 0.01 % formic acid yielded fast desolvation, high ionization efficiency, and low matrix effect which could benefit complex biological matrices analysis.

Introduction

Inert carrier, 90 % sCO₂, limits the matrix effect on electrospray ionization efficiency which is controlled in part by solvent evaporation.1 Nanospray emitters (nESI) provide small initial droplets resulting in high ionization efficiency.² Typically fast desolvation of the liquid droplet gives high transmission of the analytes into the gas phase.³ Evaluation of the ionization efficiency is challenging as the physical state of the droplet and charged ions change on a nanosecond timescale.^{4, 5} Efficient electrospray is mainly controlled by the proton affinity (PA), the surface activity, solvent polarity, desolvation, ionic transmission, the excess charge on the droplet, and droplet size.^{2,6-8} Reduction of the spraying droplet size using nanospray results in improved ionization efficiency.⁵ Substantial changes to these factors in addition to the analyte composition like hydrophobicity and ionic repulsion results in different ionization mechanism.4, 9,10

Electrospraying a supercritical fluid (SF), like carbon dioxide (sCO₂) can enhance desolvation.¹¹ It results in an increased ionization efficiency and lower background signal when used as a carrier phase compared to organic liquid phase ESI. The reduced SF matrix effect mitigates signal suppression of the analyte and thereby increases the MS signal.¹² Coupling the SF to MS using a nanoemitter (nSF-MS) has shown improved MS signal/sensitivity¹³ and can potentially provide

insights into the ionization of small molecules. Analysis of different chain lengths, polarity, and proton affinity would help evaluate the ionization from the supercritical fluid. 14, 15

In the ESI equilibrium-partitioning model,⁷ the droplet surface carries a greater fraction of the excess charge,⁸ and analytes at the surface are more likely to escape from the droplet surface.¹⁶ The limited number of excess surface charges available to the analyte(s) results in competing ionization. The ionic suppression resulting from the competition between the media and different analytes limits analyte ionization.¹⁷ The chain ejection model describes the droplet as having the analyte hydrophobic moiety out of the exterior of the droplet which yields a higher signal.² The signal increases as the hydrophobicity increases.¹² Nanospraying SF with limited matrix effect and ionic suppression potentially may unravel differences in the ionization mechanism.

Signal response in electrospray is limited by adduct formation and solvent ionization. ^{18, 19} The transfer of trace salts in the liquid solvent (e.g., Na⁺, K⁺) to the analyte during ionization results in multiple peaks formation for a single analyte. Nanospray using a capillary emitter is shown to limit adduction. ^{20, 21} Nanospraying sCO₂ further reduces adduction due to the diminished media effect.

¹Department of Chemistry and Biochemistry, Saint Louis University, 3501 Laclede Ave, St Louis, MO 63103, USA.

²Department of Chemistry and Biochemistry, Ohio University, 307 Chemistry Building, Athens, OH 45701, USA.

³Department of Chemistry and Biochemistry, Rowan University, 201 Mullica Hill Rd., Glassboro, NJ 08028, USA.

^{*} Corresponding author email: jim.edwards@slu.edu

A study on the effect of proton affinity, hydrophobicity, nano emitter i.d., modifier additives, and matrix effect on ionization is presented here to evaluate the nSF-MS performance. We use a set of primary, secondary, tertiary, and quaternary amine model compounds with butyl-, hexyl-, octyl-, and decylside chains nanosprayed by 25, 50, and 75 µm internal diameter (i.d.) capillary with emitter tip sizes of 486, 544, and 2190 nm. Signal intensity in nSF-MS was found to be dependent on the hydrophobicity and the droplet size rather than the PA. The efficient desolvation has shown analyte-dependent MS signal response. Our results provide insights to factors affecting the ionization efficiency of the supercritical fluid nanospray.

Materials and Methods.

Reagents and capillaries.

Twenty-five, fifty, and seventy-five µm i.d. (360 µm outer diameter) fused silica capillary tubes were purchased from Polymicro Technologies (Phoenix, AZ). A zero dead volume (ZDV) IDEX High-Pressure PEEK union was purchased from Cole-Parmer (Vernon Hills, IL). Fiberglass heater tapes were purchased from Omega Engineering (Norwalk, CT). A digital display PID temperature controller thermostat was purchased from Twidec (Suzhou, China).

A 300 mm Column heater "Hot Pocket", LC-MS grade water, Optima LC-MS grade methanol, formic acid, hydrofluoric acid, and ammonium acetate, were purchased from Thermo Fisher (Pittsburgh, PA). Butylamine, hexylamine, octylamine, decyl amine, N-methyl butylamine, N-methyl hexylamine, N-methyl octylamine, N-methyl decylamine, N,N-dimethyl butylamine, N,N-dimethyl butylamine, N,N-dimethyl butylamine bromide, trimethyl butylamine bromide, trimethyl butylamine bromide, and a 500 mg C18 solid-phase extraction tube SupelcleanTM LC-18 (SPE) were purchased from Sigma Millipore (Saint Louis, MO). Trimethyl decylamine bromide was purchased from Alfa Chemistry (Ronkonkoma, NY).

Capillary interfaces.

Capillary nanotip orifices were fabricated using a trap-end frit, laser-pulled method. 22 Briefly, windows were generated in a 15 cm long fused silica capillary using an electrical arc to remove the polyimide coating. Photopolymerized frits were generated using a monomer mix of 350 μL trimethylolpropane trimethacrylate and 150 μL of glycidyl methacrylate with 7.9 mg of benzoin methyl ether (BME). The porogenic solvent was prepared by mixing 250 μL toluene and 750 μL isooctane. The monomer solution (300 mL) was added to the porogen solution and sonicated for 15 minutes. The frit mixture is loaded into the capillary and polymerization was initiated with UV-lamp (UVP, Cambridge, UK): wavelength was 365 nm, time for the reaction was 30 minutes at ambient temperature.

Nanospray tips were generated using a laser fiber puller model P-2000 (Sutter Instruments, Novato, CA, USA) with a heating time 420 msec, velocity 80 msec, delay time 150 msec, and pulling time 225 msec. Each nano emitter fritted capillary was etched in 51 % hydrofluoric acid by 50 submersions in 30 seconds to open the fine tip resulting in the nanospray emitter. The 25, 50, and 75 μ m i.d. capillaries were trimmed to 2 cm. The capillary before the split was wrapped in heating tape to maintain the temperature of the SF. The short emitter, inline photopolymerized frit, and the proximate position to the MS achieved nanospray. Edited laser-pulling methods were used to create (0.50, 0.75, 1.00, and 2.00 μ m tips) on the 25 μ m i.d. emitter (Supplemental Table 1).

SEM imaging.

To determine the nanospray orifice size, scanning electron microscope (SEM) imaging was performed on the laser-cut HF-etched capillaries. They were sputter-coated with gold metal at 30 mA for 40 sec. using a vacuum chamber (Denton Vacuum LLC, NJ). The sputter-coated capillaries were imaged by an SSD camera Inspect F50 model. The SEM (FEI, Hillsboro, OR) was operated at 10 kV acceleration voltage to give the optimum image pixels. The tip size images were analyzed using the ImageJ software (National Institutes of Health, Bethesda, MD). SEM was used to image the capillary columns i.d.s and the different tip sizes (Supplemental Figure S-1).

Sample preparation.

Purification of quaternary amines.

The presence of counter-ions may result in the neutralization of the quaternary ion and salt formation.²⁴ The halide counter-ion has been shown to form complex clusters with other ionizable species in the solution.²⁵ Injection of the quaternary amines individually, has shown low analyte signal intensity and a complex mass spectrum indicating adduct formation and clustering (**Supplemental Figure S-2**). To eliminate this occurrence, the quaternary amine standards were subjected to a Solid Phase ion Exchange (SPE) cartridge to remove the bromide ions. Twenty mM of each quaternary amine stock solution was purified by the C18 SPE column. 2.5 mL of water was used for conditioning the SPE particles. 1 mL aliquot of each quaternary amine was injected through the SPE extraction tube separately. Rinsing of the standards retaining on the SPE column was performed using 1 mL H₂O to remove salts followed by a 1 mL CD₃OD for quaternary amines elution.

The recovered extracts were dried separately at room temperature under a vacuum centrifuge. The dried extracts were reconstituted in 1 mL CD₃OD and spiked with 200 mM formic acid internal standard for quantification. This was done using quantitative nuclear magnetic resonance (qNMR) experiments. After quantification of the purified stock standard solutions, samples were dried again in the vacuum centrifuge at room temperature and reconstituted in methanol.

Nuclear Magnetic Resonance.

Bruker Advance HDTM 700 MHz NMR spectrometer was used for quantification of the C18 SPE-purified quaternary amines in qNMR scans. Relative concentration quantification was done using the formic acid internal standard. The adjusted parameters for qNMR data acquisition were: the relaxation time (T1) = 7.77 sec = 1.44 Tnull, the relaxation delay time (D1) = 50 sec, acquisition time (taq) = 5.19 sec, the 90 °pulse = 8.725, and the RsFID = 0.19 Hz. The scanning rate was 19 sec/1scan which gave the signal to noise of (S/N = 82,859). NMR spectrums of the purified quaternary amines are shown in (Supplemental Figures S3 – S6).

Stock and working solutions.

10 mM standard stock solutions of the primary, secondary, tertiary, and purified quaternary amines were prepared. A separate $50~\mu M$ primary, secondary, tertiary, and quaternary working solutions each of butyl-, hexyl-, octyl-, and decyl- amines were prepared in methanol with 0.1 % formic acid. A mixture of octylamine, N-octylamine, N,N-dimethyl octylamine, and trimethyl octylamine were prepared at different concentrations of (100 nM, 1, 10, 50, and 100 μM) for the competing ionization study.

Supercritical fluid system.

Shimadzu's 'Nexara UC' supercritical fluid system is driven by a modifier pumping (LC-30A) and CO₂ solvent delivery unit LC-30ADSF system. The CO₂ gas delivery unit has a built-in pump head cooler and uses a micro-volume double plunger pump. The

system contains a communication bus module (CBM-20A) and (SIL-30AC) autosampler. The temperature was controlled by (CTO-20AC) heating oven and the pressure was controlled by an SFC-30A back pressure regulator (BPR).

Mass Spectrometer.

Experiments were performed on an LTQ XL Linear Ion Trap mass spectrometer (Thermo Fisher Scientific, San Jose, CA). A Thermo nanospray FlexTM ion source emitter in positive ionization mode was used for the characterization of the nanospray at +1-4 kV spray voltage, 250 °C capillary temperature. A Thermo source ESI housing heated probe (HESI) was used for full flow sample introduction. The optimized parameters were as follows: sheath gas was 10, auxiliary gas was 7, sweep gas was 5, and spray voltage was 3 kV. The capillary temperature was 250 °C. The mass range was from 50 - 300 m/z, scan time was 1 micro-scan, maximum injection time 10 msec, and AGC was 1E6.

Data Processing: Xcalibur, GraphPad Prism, and RStudio.

Data files in (.RAW) format were displayed on Xcalibur Qual browser software from Thermo Scientific. Graphing was done using GraphPad Prism9 software. The 3D heat maps of signal intensities as a function of pressure and volumetric flow rates were displayed using RayShader. It is an open-sourced 3D mapping package using 'R' software. R is programming and displaying software using the RStudio platform.²⁶

Computational estimates of proton affinities.

Simulations were performed to enable effective characterization of the potential energy surfaces of the neutral and protonated amines. Candidate structures were systemically generated via the tool Fafoom, a genetic algorithm.²⁷⁻³⁰ The structures were initially optimized using the MMFF94 Force Field.³¹ Geometry optimizations of the resulting candidate conformations were performed with the Gaussian16 software package at the M06-2X/6-31+G(d,p) and then M06-2X/6-311++G(2d,2p) levels of theory.³² Degenerate structures were removed between stages. Frequency calculations from the optimized structures enabled the standard enthalpy at 298 K to be calculated. Our computational estimates of

the proton affinities of the neutral analytes were determined as the difference between the lowest standard enthalpy at 298 K values of the protonated analyte, and the sum of the neutral analyte plus the 6.2 kJ mol⁻¹ correction for the thermal energy of a proton at 298 K.³³

Results and discussion.

System optimization.

The nSF-MS system was used to evaluate the signal response for analytes of different proton affinities and hydrophobicities (Figure 1). Nanospraying a set of butyl-, hexyl-, octyl-, and decyl- side chains of the primary, secondary, tertiary, and quaternary amines separately for each amine class was done using 90 % sCO₂ with 9.99% methanol (0.01 % formic acid final concentration) as a carrier phase. The 3D heat maps show the MS signal response as a function of the back pressure regulator (BPR) in (MPa) and the linear velocity of the effluent in (cm/sec). A clean MS spectrum with low background noise was observed across different operating conditions. This may be due to the efficient desolvation of the ionizing media nanospraying the SF effluent. 13 To ensure that carbamates are not formed between the amines and sCO2, we monitored for the potential product and observed no indication of this reaction (Supplemental Figure 7) at 50 °C in $\sim 0.3 - 0.5$ seconds elution time (Supplemental Figure S-24, S-26). 34,35

Nanospraying longer alkyl chains showed higher signal response across all amine classes. This observation was most pronounced in the quaternary amines. As there is no proton/charge transfer step to the ionization process for quaternary amines, the higher signal is a result of the hydrophobic moiety increasing surface location. This likely occurs due to the increase in solvophobicity. ¹⁴ The increased hydrophobicity may have resulted in increased dispersion in the carrier phase which increases the readiness of the molecules to leave the electrospray droplet. This ultimately improves the MS signal response.

Based on these initial results, the system was further tested to examine the scope of changing SF and flow-based parameters. The system was designed to maintain the supercritical state until

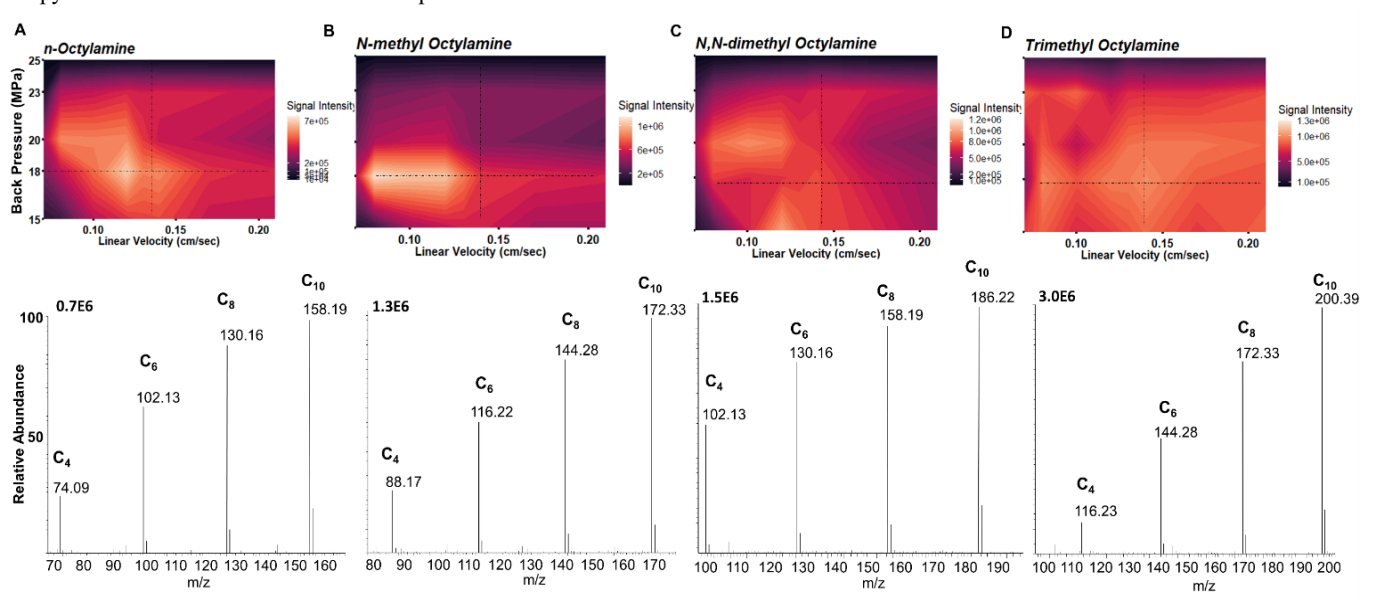


Figure 1: Optimization of the operation pressure and the linear velocity of the supercritical fluid-nanospray-MS (nSF-MS) signal response. 3D heat map signal intensity trends as a function of pressure (MPa) and linear velocity (cm/sec) and the corresponding MS spectrum nanospraying supercritical fluid A) primary, B) secondary, C) tertiary, and D) quaternary octyl amines and the MS spectrum of butyl- (C₄), hexyl- (C₆), octyl- (C₈) and decyl (C₁₀) hydrophobic side chains of each amine class using 75 μm i.d. nano emitters.

reaching the emitter orifice. 13 System optimization was performed using laser-pulled HF-etched inline embedded photopolymerized frit 2 cm nanoemitters. The split flow emitters resulted in 64, 174, and 352 nL/min using the 25, 50, and 75 µm i.d. respectively. This was done at the pressure range of 15 – 25 MPa using 50 °C heated connections nanospraying sCO2 with 10 % methanol (0.01 % formic acid) at 3 kV.13 Investigation of the amines signal response was a function of the linear velocity of 0.15 - 0.42 cm/sec for the 25 um, 0.14 - 0.40 cm/sec for the 50 um, and 0.07 - 0.21 cm/secfor the 75 µm i.d. nano emitters (Supplemental Figures S8 – S19). The primary, secondary, and tertiary amines showed an increasing nSF signal response as the volumetric flow rate increased from 0.15 - 0.40 for the 25 μm i.d., 0.14 - 0.38 μm i.d. for the 50 μm i.d., and 0.07 - 0.17 cm/sec for the 75 μ m i.d. The signal intensity started to drop flowing faster than 0.40, 0.38, and 0.17 cm/sec for the 25, 50, and 75 µm i.d. respectively. Low to non-detectable signal response was found when flowing slower than 0.15, 0.14, and 0.07 cm/sec for the 25, 50, and 75 µm i.d. respectively (data not shown). The highest signal was found at 0.28, 0.26, and 0.14 cm/sec for the 25, 50, and 75 µm i.d. respectively using 90 % sCO₂ at 18 MPa, 50 °C.

The SF density and the operating pressure is determined in part by the percent methanol present. 36 A minimal amount of methanol was used to achieve a stable MS signal response and explore the effects on ionization. The effect of methanol on MS signal response and the pressure of the operating pumps is shown in **Supplemental Figure S-20** and **Supplemental Table T-2**. Increasing the % methanol from 5-10 % has shown a linear signal intensity and pressure increase. Exceeding the 10 % modifier has shown a slight signal drop while the pump pressure continues to increase. Beyond 50% methanol, density errors from the pump ensued, likely due to the high flowrate and combination of the restrictive nanospray system. 36 , 37 , 38

Ionizing media effect.

Modifier additives (e.g. water, salts) have been used to enhance sensitivity and improve selectivity in supercritical fluid chromatography.³⁹ **Figure 2** shows the modifier effect on the primary, secondary, tertiary, and quaternary amines signal using a 75 μm i.d. open tube nSF emitter with a tip size of 2190 nm. A 1 μL injection of each amine class was performed individually to investigate the modifier additives effect. Formic acid showed a significant improvement in the nSF-MS signal response compared to pure methanol for all amine classes. While the pKa of the sCO₂:CH₃OH mixture is unknown, the apparent pH was experimentally found around 5 - 6.³⁷ Increasing the acidity using formic acid increases proton availability and ionization efficiency.⁴⁰ However, a full

investigation of the role of the pH on the MS signal response was not covered in this study. The formic acid effect on the nSF signal response was less pronounced in the quaternary amines. This is due to the fixed positive charge where desolvation of the quaternary amines is the driving force to gas phase ionization, irrespective of the ionizing media. 41, 42 The signal enhancement of quaternary amines with the addition of formic acid is likely due to increased conductivity of the fluid.

Ammonium acetate and water have been used in SF systems to enhance chromatographic performance. ^{43, 44} These salts and water showed signal suppression effects on the amine signal in our nSF-MS open tube system in the form of adduct peaks (**Supplemental Figure S-21**) as previously reported. ¹⁸ This may explain the signal drop using ammonium acetate or water additives.

Methanol acidifies the sCO₂ and enhances the carrier polarity.³⁷ Decreasing the pH using formic acid spiked into the methanol has shown improved MS response. A similar observation was found for the quaternary amines signal. The acidic media should decrease the counter ions, thereby enhancing the availability of free quaternary amines.⁴² Increasing the basicity of the modifier has shown signal suppression of the amines. In such a case, the modifier gets protonated at the expense of the amines which may be attributed to adduct formation or signal suppression effects.^{12, 15} The complete understanding of the effect of pH would be interesting for future studies.

Competing Ionization.

The ionizing media typically acquires a charge more readily than the analyte, competes with it, and results in signal suppression. The polar moiety of the analyte eases ionization whereas the hydrophobic moiety gives a higher signal response. 14 A 1 μL mixture of primary, secondary, tertiary, and quaternary amines was injected at different concentrations. **Figure 3A** shows the MS spectrum of the octyl amines mixture where the base peak of the quaternary octyl amine was found. The relative abundance of the tertiary amine was 50 % whereas the primary and secondary amines were between 15 – 25 %.

This further supports the observed detection sensitivity based on the charge transfer step in achieving gas phase ionization. Injection of a mixture of primary, secondary, tertiary, and quaternary octyl amine mixture (Figure 3B) was done to compare the competing ionization versus injection of quaternary octyl amine injection alone (Figure 3C). These injections were done at different concentrations separately. The quaternary octylamine signal intensity was statistically the same whether injected alone or in a primary,

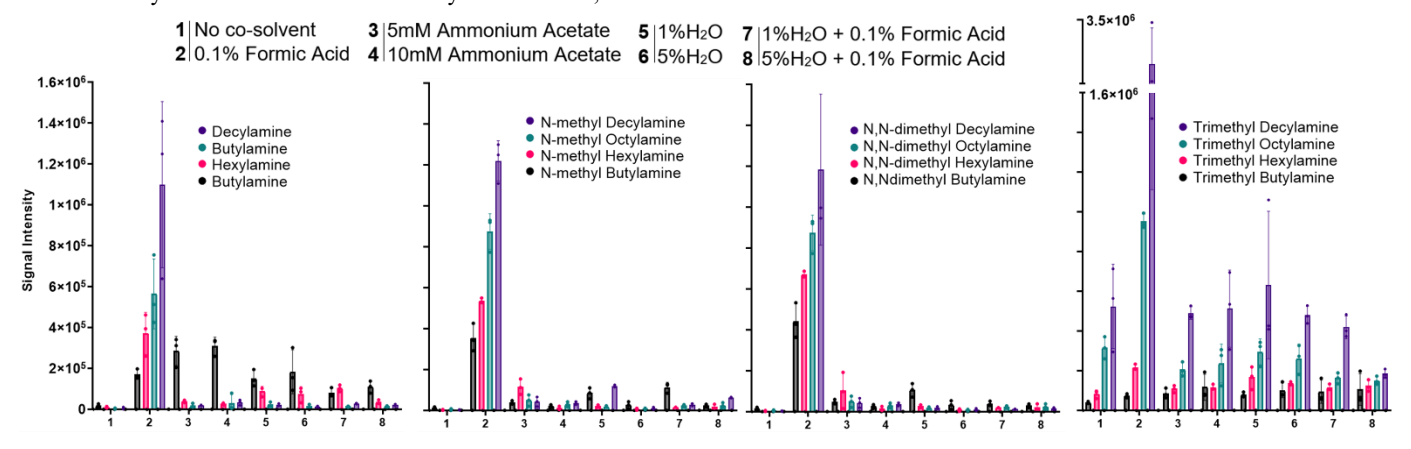


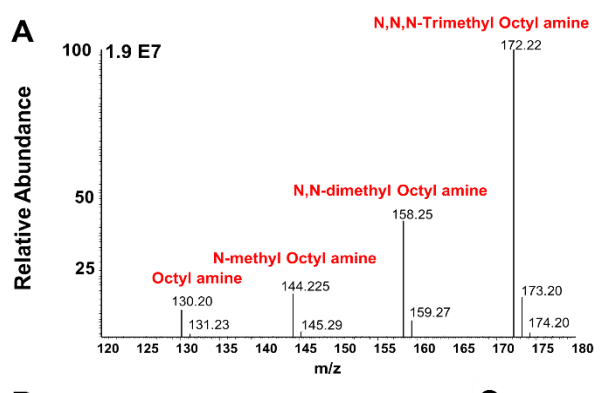
Figure 2: Modifier additives effect on nSF-MS signal response. The nSF-MS signal intensities of A) primary, B) secondary, C) tertiary, and D) quaternary amine mixtures using the 75 μm i.d. interface at 18 MPa, 50 °C, 0.14 cm/sec using 90 % sCO₂: 10 % methanol spiked with co-solvents 1 – 8 added to the methanol.

secondary, tertiary, and quaternary octyl amines mixture. These results indicate that the quaternary amines electrospray had minimal signal suppression with either solvent or ionizable species in the injected sample plug.

Competing ionization was found between the primary, secondary, and tertiary amines. The tertiary amines showed a higher signal intensity than the secondary and primary amines on a dynamic range of $0.1 - 100 \mu M$. Results indicated competing ionization depends on the concentration of the ionizing species. 17,46 Increasing the sample concentration was followed by a more pronounced competing ionization effect.¹⁷ The quaternary amine signal was slightly higher than the other amines in the 100 nM sample. The signal intensity difference between the quaternary and the other amines increased with concentration increase. Ten-fold higher signal intensity was found for the quaternary octylamine compared to the primary and the secondary octylamines between $25 - 100 \mu M$. The tertiary octylamine signal was statistically higher than the primary and secondary amines and lower than the quaternary amine. Ultimately, the primary, secondary, and tertiary amines yield signal responses that are most similar at lower concentrations compared to higher concentrations.

A linear relationship with R^2 of 0.998, 0.999, 0.998, and 0.998 was found for the primary, secondary, tertiary, and quaternary amines respectively to the dynamic range of $0.1-100~\mu M$ (Supplemental Figure S-22). Collectively, the quaternary amine yielded a higher response over all the other amines whereas the tertiary amine outcompeted the primary and the secondary amines. Agreeing with our previous study on the nSF system development, 13 injections of amines have shown mass-sensitive detection (Figure 3D). When the MS signal response changes linearly with increasing the mass injected, the detection sensitivity is considered mass-sensitive. 47 Injection of 1, 2, and 5 μ Ls of primary, secondary, tertiary, and quaternary octylamines separately have shown a signal intensity increase. A significant signal intensity gain was found in nanospraying the quaternary amine as the mass injected increased, indicating a high degree of desolvation.

Interfacing the SF to the MS is typically performed using a makeup flow. 48 It is used to avoid precipitation as solubility drops as a function of the CO2 depressurization during chromatographic elution. 49 However, this results in sample dilution, ionic suppression, and sensitivity loss. $^{12,\,13,\,50}$ Methanol with 0.1 % formic acid flowing at 0.2 mL/min was used as makeup to 1 mL/min 90:10 sCO2:CH3OH (0.01 % formic acid) supercritical fluid using a 75 μm i.d. emitter. The makeup flow resulted in a signal intensity drop for all the amine classes tested (Supplemental Figure S-23). The introduction of organic makeup flow to the supercritical fluid resulted in a signal intensity drop whereas the nSF-MS split-flow resulted in signal intensity enhancement. It showed signal intensity



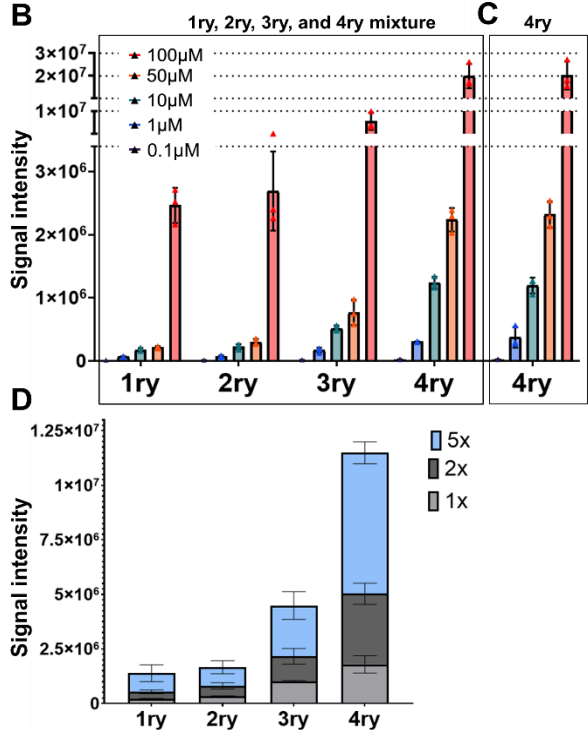


Figure 3: Competing ionization and MS detection sensitivity nanospraying 90 % supercritical fluid CO₂. A) MS spectrum of 100 μM octyl amines. The nSF-MS signal intensities of B) primary (1ry), secondary (2ry), tertiary (3ry), and quaternary (4ry) octyl amines mixture and C) 4ry octyl amine only using a 75 μm i.d. emitter at 18 MPa, 50 °C, 0.14 cm/sec. D) Mass-sensitive nSF-MS signal intensity trends shown by 1, 2, and 5 μL injection volumes.

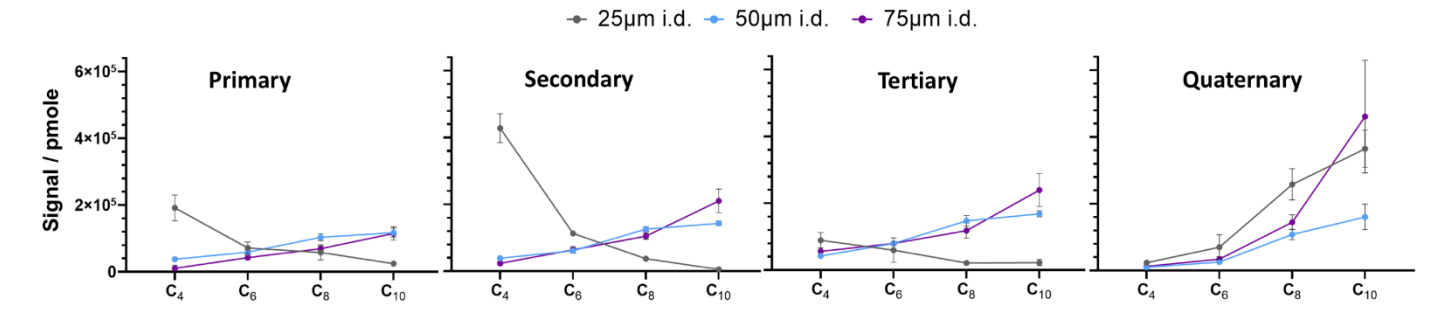


Figure 4: Emitter tip size effect on the MS signal of the supercritical fluid nanospray. The MS signal intensity trends of A) primary, B) secondary, C) tertiary, and D) quaternary; butyl (C₄), hexyl (C₆), octyl (C₈), and decyl (C₁₀) amines. The amines were nanosprayed by 90 % sCO2: 10 % methanol (0.01 % formic acid) using 25, 50, and 75 μm i.d emitters.

gain of $2.13 \times 10^5 \pm 1.9$ for the primary amines, $4.5_2 \times 10^5 \pm 0.2$ for the secondary amines, $4.05 \times 10^5 \pm 0.3$ for the tertiary amines, and $6.7_9 \times 10^5 \pm 0.6$ for the quaternary amines.

Nanoemitter tip.

Nanoemitters with low to sub-micron tip diameters produce a small droplet size improving the ionization efficiency.⁵¹ They diminish analyte-salt adduction during droplet evaporation and result in enhanced MS detection.⁵² Figure 4 shows a normalized signal intensity comparison of nSF for all the amine classes injected separately. Because the system operates in mass sensitive detection, ¹³ signal intensity was normalized to mass injected (1.16, 3.16, and 6.40 pmoles for the 25, 50, and 75 µm i.d. emitters respectively). The quaternary amines show an increased signal intensity trend as hydrophobicity increased throughout all the emitter i.d.s and tip sizes.⁵³ However, in a mass-sensitive detection, a comparable signal response was found amongst different amine classes after normalization to the mass injected. This indicates the substantial effect of proton transfer in the nanospray of supercritical fluids. For 75 and 50 µm capillaries with 2 µm and 0.5 µm tip orifices respectively, the increase in alkyl chain length corresponded to an increased signal response. This did not hold for the 25 µm capillary with a 0.5 µm tip orifice. The inverse was observed, as increased chain length showed a decrease in signal amongst primary, secondary, and tertiary amines. Because the tip orifice (0.5 µm) is the same for both 25 and 50 µm capillaries, the substantial difference is likely attributed to the flow rate as shown in the **Supplemental** Figure S-24 FIAgrams. Examination of the same nanospray emitters using conventional organic solvent instead of SF did not show such trends at the 25µm emitter (Supplemental Figure S-25).

The decrease in signal response as alkyl chain length increased for the 25 μ m i.d. (~500 nm) emitter was of distinct interest. To investigate the observation of decreasing signal intensity with increasing alkyl chain length, 0.5, 0.75, 1.0, and 2.0 μ m tips were laser-pulled on 25 μ m i.d. emitters (**Figure Table T-1**). Injection of 1 μ L of 50 μ M of each amine class was done individually on each emitter. The apparent signal intensity was normalized to the mass injected of 1.16, 2.13, 4.33, and 5.65 pmoles injected on a 0.5, 0.75, 1.0, and 2.0 μ m emitter on the 25 μ m i.d. emitter

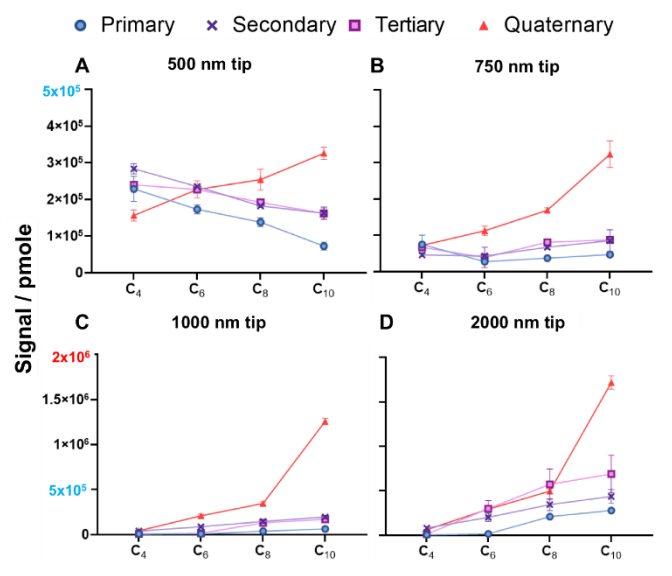


Figure 5: Characterization of the effect of tip size on nSF signal response. Normalized signal response and picomoles injected using A) 0.50 μ m (1.16 pmole), B) 0.75 μ m (2.13 pmole), C) 1.00 μ m (4.33 pmole), and D) 2.00 μ m (5.65 pmole) tip size on the 25 μ m i.d. nESI emitter.

respectively. The primary, secondary, and tertiary amine signal reduction with increasing hydrophobicity was consistent with using the 486 nm tip (Figure 5).

The decrease in signal intensity with increasing chain length in the 500 nm tip is contrary to conventional understanding.¹⁴ The phenomenon is possibly due to an alteration of the electrospray mechanism at small droplet sizes.^{2, 14, 54} The small initial nano droplet consisting of 90% evaporative sCO2 and 10% methanol may have resulted in substantial and rapid desolvation which largely depends on the ionic repulsion between the charged analyte and the aerosol droplet.^{2,54} The smaller ions would have had higher ionic repulsion from the ionic droplet. This results in higher ionic transmission and consequently higher signal for the smaller analytes. ^{2, 5, 55} Another factor that may have attributed to the difference in sensitivity is the desolvation time of different structures of the ionizing species.^{2,7} The 25 µm i.d. with a 500 nm emitter may not provide enough time for transferring the charge onto the analyte before the analyte is ejected.^{5,56} In this case, the larger hydrophobic molecules may be squeezed out of the droplet rapidly as neutrals before they have time to be protonated.

As the tip i.d. increased for the 25 μ m i.d. emitter, the inverse signal intensity to the hydrophobicity effect was mitigated for those analytes requiring proton transfer. The flow rates for 500 and 750 nm orifices were nearly identical yet showed distinct responses for increasing alkyl chain lengths (Supplemental Figure S-26). The 0.5 μ m showed a decrease in signal with increasing chain length while the 0.75 μ m showed no substantial change in signal response with hydrophobicity. Because the flow rates were near equivalent for both tips, the differences in signal response are attributed to orifice size.

An overall decrease in signal intensity was found for the primary, secondary, and tertiary amines when the emitter tip is increased to 0.75 and 1.00 μm (Figure 5, y-axis red and blue). The signal from the quaternary amines was relatively similar when nanosprayed on the 0.5 and 0.75 μm tips of the 25 μm i.d. emitters. Of considerable interest is the 0.75 μm emitter tip response. In this case, a near plateau of signal intensity is found for changes in the alkyl chain length. This also holds for the level of amine methylation. Although limited in the number of analytes, these trends hold the possibility of generating near-equivalent signal responses independent of hydrophobicity and amine methylation/proton affinity. This contrasts with the increasing slope of signal intensity and chain length found using the 1 and 2 μm tips.

The results from **Figure 4** show that the flow rate dictates the differences in the signal response of alkyl chain length. **Figure 5** indicates that on small flowrates, orifice size dictates the response of alkyl chain lengths. Taken together, these results suggest that both flow rate and orifice size are critical to understanding this new phenomenon. More studies are needed to further clarify the situation.

Ionization efficiency.

The ESI ionization is largely dependent on the PA of the desolvating analytes. ⁸ Ionic suppression may be evolved if the PA_{analyte} < PA_{solvent}. Computational estimation of the gas-phase PA of the primary, secondary, and tertiary amines using the M06-2X/6-311++G(2d,2p) level of theory (Supplemental Table T-3) indicates a systematic increase from 917.0 kJ mol $^{-1}$ (Butylamine) with size and degree of nitrogen substitution consistent with earlier work on smaller systems. $^{27,\,32}$

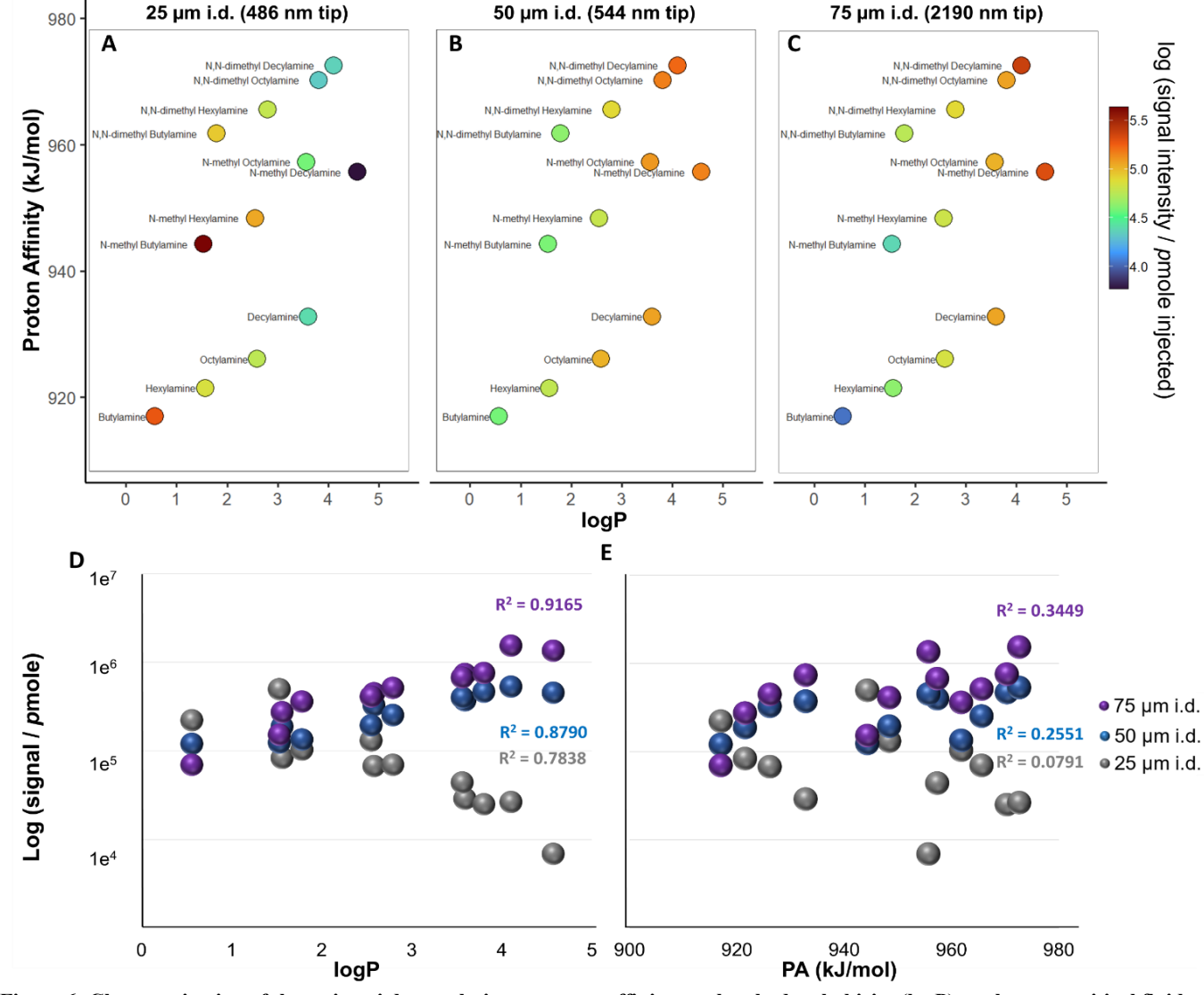


Figure 6: Characterization of the emitter i.d. correlation to proton affinity, analyte hydrophobicity (logP) on the supercritical fluid-nanospray-MS (nSF-MS) signal response. Signal intensity trends and the corresponding ionization efficiency nanospraying supercritical fluid on a A) 25, B) 50, and C) 75 μ m i.d. emitter. The log (normalized amine signal to number of picomoles injected) is color-scales from 4 -5.5 as the deeper red represents a higher signal and deeper blue represents lower normalized signal. Logarithmic scale normalized signal per picomoles injected as a function of D) logP and E) proton affinity (PA) (kJ/mol). The decreasing 25, and increasing 50, and 75 μ m i.d. nano emitters signal intensity trends as a function of analyte hydrophobicity (logP). The normalized values were 1.16, 3.16, and 6.40 picomoles injected on the 25, 50, and 75 μ m i.d. nano emitters respectively.

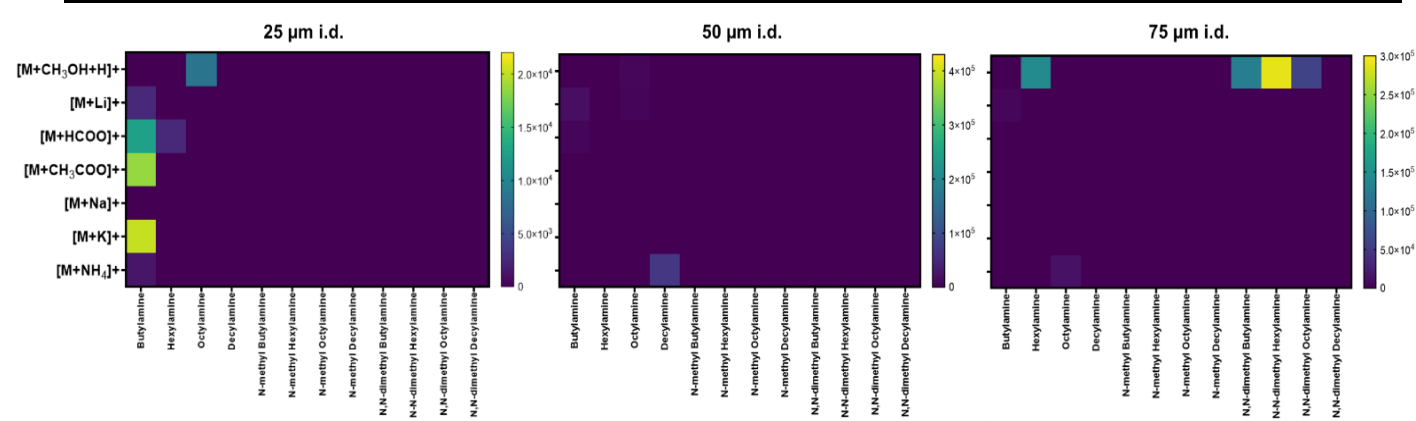


Figure 7: Adducts profile of organic liquid and supercritical sCO₂ carrier nanospray. Comprehensive adduct peaks signal intensities nanospraying supercritical fluid (nSF) for primary, secondary, and tertiary amines with butyl-, hexyl-, octyl-, and decyl hydrophobic side chains.

While the PA_{90%sCO2} with 10 % methanol (0.1 % formic acid) is not known, PA_{CO2} and PA_{CH3OH} are 540.5, and 754.3 kJ/mol respectively.⁵⁷ Results have shown an increased signal intensity as the proton affinity increased by the order of tertiary > secondary > primary (**Supplemental Table T-3**).⁴⁶ Normalization to the mass injected has shown a comparable signal response to different amine classes on the same emitter i.d.

Contrasting the calculated PA with the nSF-MS signal response was done after normalization to the 1.16, 3.16, and 6.40 pmoles injected on the 25, 50, and 75 μm i.d. emitters respectively for each amine class (Figure 6 A-C). Results show increasing trends for 50 and 75 μm i.d. emitters as a function of logP (warming colors). A decreasing signal intensity trend were found using the 25 μm i.d. emitter as the logP increased (cooling colors). The small emitter (tip size \sim 486 nm) (Supplemental Figure S-1) likely produced extremely small initial droplets. Nanospraying 90 % sCO2 using a nano-scale emitter resulted in a difference in which the ionization mechanism dominated the event.

Ionization efficiency depends on the initial droplet size, logP, and the nature of the analyte for conventional nanospray systems.^{1, 2} **Figure 6D, E** show the averaged normalized signal intensity of primary, secondary, and tertiary amines as a function of logP and PA. Our results have shown a linear correlation of the nSF-MS signal towards the logP and a non-linear correlation for PA. The 25 µm i.d. emitter has shown decreasing signal trends as a function of logP and PA.

These results suggest a correlation of the analyte hydrophobicity to the ionization efficiency more than the PA in the nSF-MS system. The efficient ionization may have been attributed to near-complete desolvation and increased ionization opportunity for analytes of different proton affinities. This led to ionization independent of the media and a more pronounced tip size effect. Increasing the hydrophobicity of the alkyl side chain seemed to largely affect the ionization mechanism across all emitters. ^{53, 58} The quaternary amines have shown signal response unaffected with the emitter tip size but increasing as logP increases. This may be explained by the quaternary amines acting as weak Lewis acids which weakly interact with the solvent. ⁴² They are being repelled from the charged droplet which results in desolvation almost independent of the presence of ionizable species. The fixed positive charge may have resulted in MS detection controlled by desolvation of the hydrophobic moiety rather than proton affinity. ^{45, 59}

Adduct profiling.

Analytes [M] are prone to adduction to ions in solution during the ESI process.⁶⁰ This results in the formation of multiple peaks of the same analyte (i.e. [M+H]⁺ and [M+ion]⁺) diminishing the analyte signal. Capillary nano emitters improve ionization efficiency, enhance sensitivity, and limit adduction.^{21, 60, 61} A systematic adduction profile of the nSF system is shown in Figure 7 for primary, secondary, and tertiary amines. A mixture of butyl-, hexyl-, octyl-, and decyl- amine of each class was injected individually using the 25, 50, and 75 µm i.d. emitters. Detailed signal intensities of the detected adduct peaks are shown in Supplemental Figures S27 – S30. The ESI process involves the acceleration of the analyte-metallic adduction. 62 This results in the formation of more adducts of the same analyte. The use of nano emitter results in limits the metallic adduction. The signal intensity of the amines adducts decreased as the nano emitter id. decreased.²⁰ Increasing the analyte hydrophobicity has shown a slight decrease in the number of adducts formed. This may be due to the increased gas-phase basicity, surface activity, and consequently ionization efficiency. 63 The nSF system showed fewer adducts which may be due to the low methanol percentage in the droplet, less organic interferent counter ions, and other alkali metal adducts. ^{14,64} The system provides enhanced sensitivity, especially in complex matrices.⁶⁵ The efficient nSF desolvation using 90:10 sCO₂:CH₃OH with 0.01 % formic acid may have provided a better ionization, desolvation, ionic transmission, and a small number of adduct peaks.

Conclusion.

The developed nSF-MS system has shown high detection capability for analytes with different proton affinities and alkyl chain lengths. $^{66,\,67}$ A linear dynamic range was found between $0.1-100\,$ μM . Competing ionization was absent for the quaternary amines whereas near-equal ionization opportunities were found for primary, secondary, and tertiary amines. The clean MS spectrum with low to no adduct peaks showed that nanospraying 90 % sCO₂ would potentially advance the detection sensitivity in complex biological matrices.

Results suggest that the nSF is largely dependent on logP and the droplet size rather than the PA. Nanospraying the SF using a 25 μm i.d. emitter (486 nm tip) has shown a signal intensity with less dependence on the analyte logP. 55 We hypothesize that the observed phenomena may be due to the difference in ionization mechanism or insufficient desolvation time. The definitive answer requires modeling of the supercritical fluid nanospray in a future study.

ASSOCIATED CONTENT

Supporting Information

The Supporting Information is available free of charge on the ACS publications website.

SEM images of 25 μm i.d. emitter, MS spectrum before and after SPE quaternary amines cleanup, qNMR of quaternary amines, MS spectrum showing the absence of carbamates, 3D signal intensity heatmaps of the primary, secondary, tertiary, and quaternary amines as a function of pressure and linear flow rate using 25, 50, and 75 μm i.d. nESI interface, modifier percentage effect on pressure and the nSF-MS signal, modifier additives effect on the nSF-MS signal, linear correlation between the nSF-MS signal and concentration, comparison between nSF and SF makeup flow, The 25, 50, and 75 μm i.d. emitters elution FIAgrams, The 25 μm i.d. emitter orifice elution FIAgrams, adduct profiling of the nSF, laser methods for nano emitters, calculated proton affinities of neutral amines, nSF pumps pressure change as a function of flow rate.

AUTHOR INFORMATION

Corresponding Author

* James L. Edwards - Department of Chemistry and Biochemistry, Saint Louis University, 3501 Laclede Ave, St Louis, MO 63103, USA. http://orcid.org/0000-0003-1063-7518

Authors

Mahmoud Elhusseiny Mostafa - Department of Chemistry and Biochemistry, Saint Louis University, 3501 Laclede Ave, St Louis, MO 63103, USA. https://orcid.org/0000-0001-7688-1789

Madisyn M. Hayes - Department of Chemistry and Biochemistry, Ohio University, 307 Chemistry Building, Athens, OH 45701, USA.

James P. Grinias - Department of Chemistry and Biochemistry, Rowan University, 201 Mullica Hill Rd., Glassboro, NJ 08028, USA. https://orcid.org/0000-0001-9872-9630

Benjamin J. Bythell - Department of Chemistry and Biochemistry, Ohio University, 307 Chemistry Building, Athens, OH 45701, USA. mh844020@ohio.edu. https://orcid.org/0000-0002-3703-0751

Author Contributions

Mahmoud Elhusseiny Mostafa: Methodology, Data curation, Formal analysis, Writing –review & editing. Madisyn M. Hayes, Methodology, Data curation, Formal analysis, Writing –review & editing. James P. Grinias: Conceptualization, Funding acquisition, Writing-review & editing. Benjamin J. Bythell: Conceptualization, Supervision, Writing –review & editing. James L. Edwards: Conceptualization, Funding acquisition, Supervision, Writing –review & editing.

Notes

The authors declare no competing financial interests.

ACKNOWLEDGMENT

This work was supported by funding from the National Science Foundation to J.L.E. (CHE-1904919), division of chemistry to B.J.B. (CHE-1948611), and directorate for mathematical and physical sciences to J.P.G. (CHE-1904454).

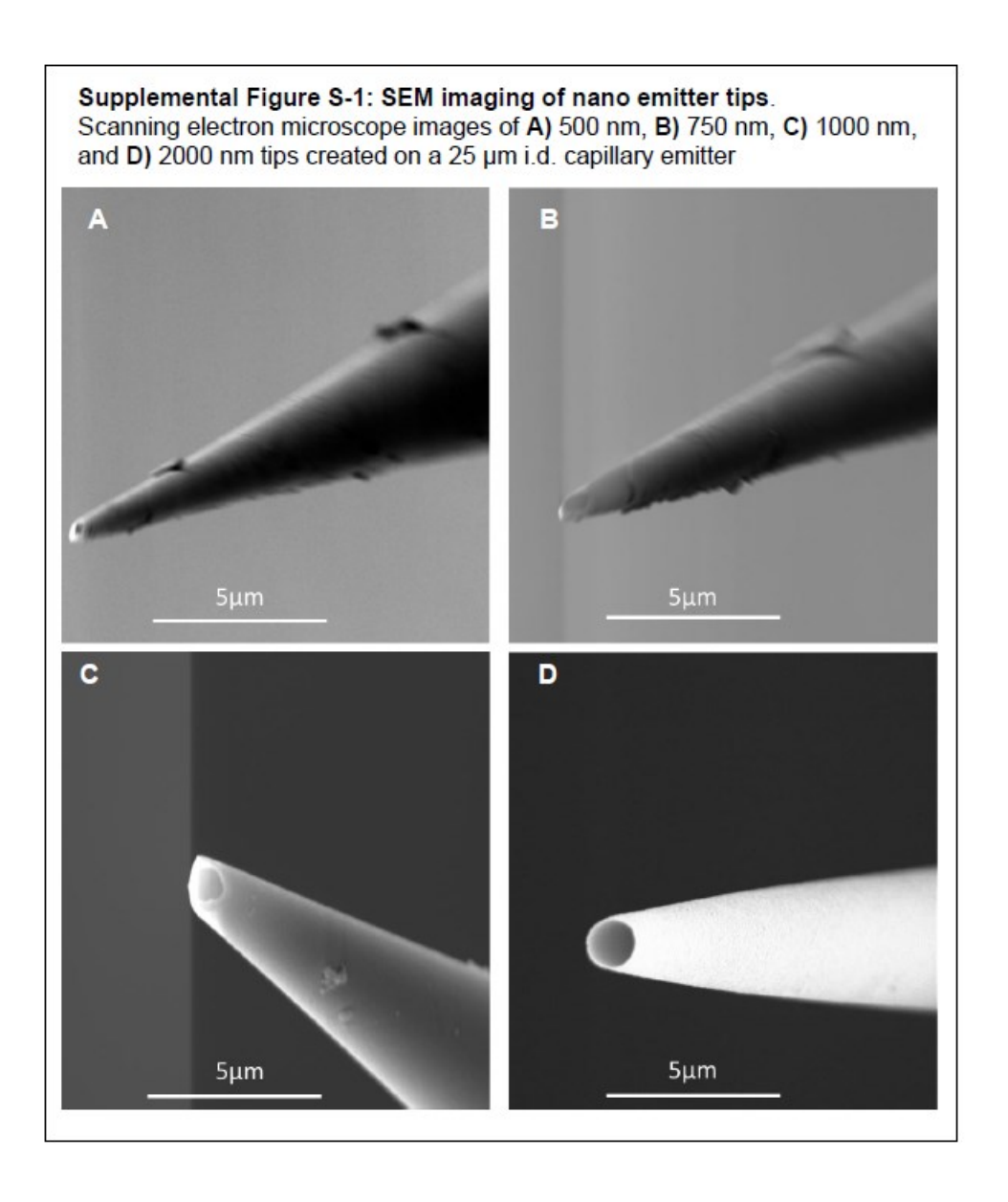
REFERENCES

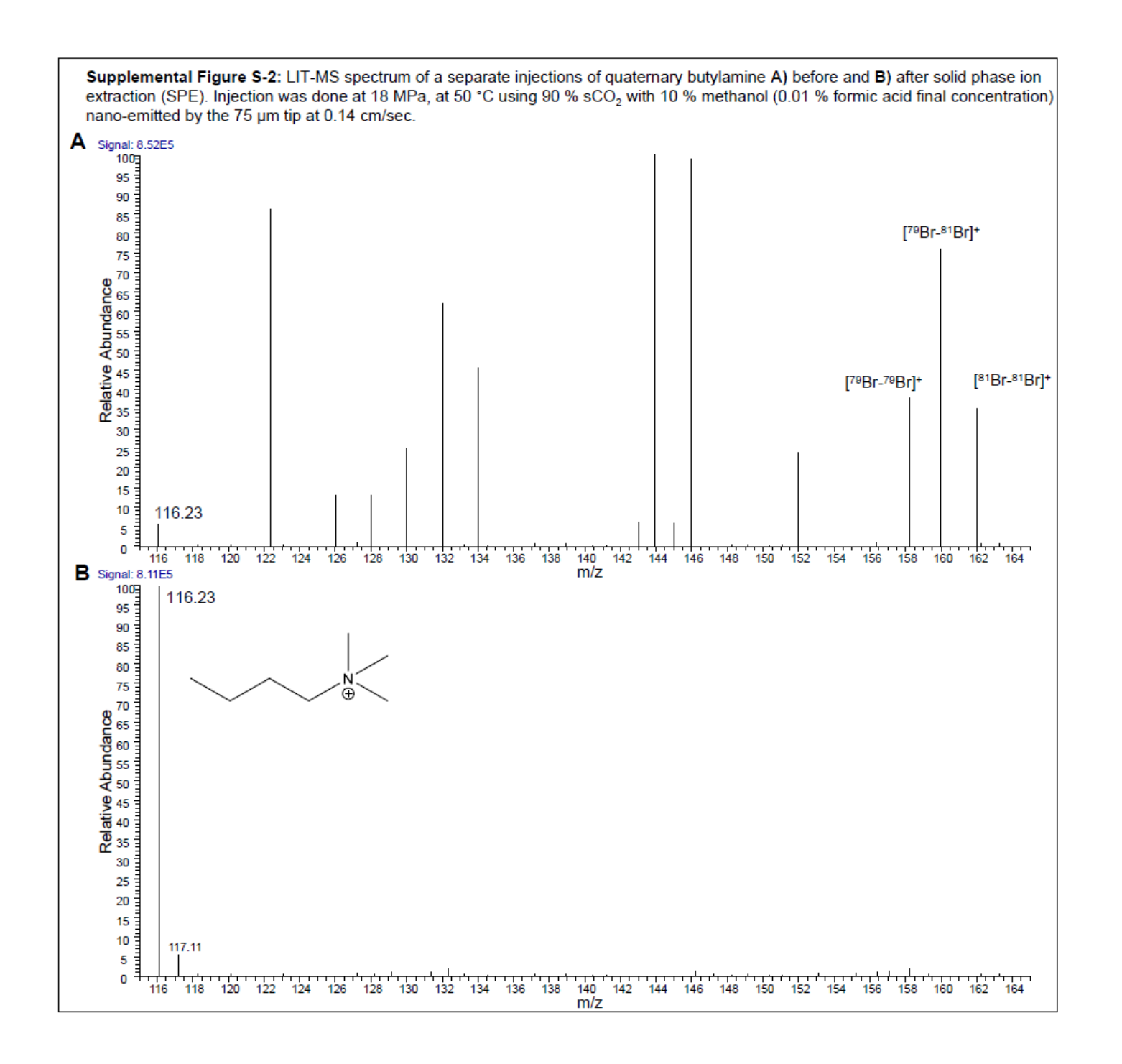
- 1. Wilm, M., Principles of Electrospray Ionization. Molecular & Cellular Proteomics 2011, 10 (7).
- 2. Konermann, L.; Ahadi, E.; Rodriguez, A. D.; Vahidi, S., Unraveling the Mechanism of Electrospray Ionization. Analytical Chemistry 2013, 85 (1), 2-9.
- 3. Bruins, A. P., Mechanistic aspects of electrospray ionization. Journal of Chromatography A 1998, 794 (1), 345-357.
- 4. Konermann, L.; Metwally, H.; Duez, Q.; Peters, I., Charging and supercharging of proteins for mass spectrometry: recent insights into the mechanisms of electrospray ionization. Analyst 2019, 144 (21), 6157-6171.
- 5. Kebarle, P.; Verkerk, U. H., Electrospray: From ions in solution to ions in the gas phase, what we know now. Mass Spectrometry Reviews 2009, 28 (6), 898-917.
- 6. Amad, M. a. H.; Cech, N. B.; Jackson, G. S.; Enke, C. G., Importance of gas-phase proton affinities in determining the electrospray ionization response for analytes and solvents. Journal of Mass Spectrometry 2000, 35 (7), 784-789.
- 7. Cech, N. B.; Enke, C. G., Practical implications of some recent studies in electrospray ionization fundamentals. Mass Spectrometry Reviews 2001, 20 (6), 362-387.
- 8. Ehrmann, B. M.; Henriksen, T.; Cech, N. B., Relative importance of basicity in the gas phase and in solution for determining selectivity in electrospray ionization mass spectrometry. Journal of the American Society for Mass Spectrometry 2008, 19 (5), 719-728.
- 9. Yuill, E. M.; Sa, N.; Ray, S. J.; Hieftje, G. M.; Baker, L. A., Electrospray Ionization from Nanopipette Emitters with Tip Diameters of Less than 100 nm. Analytical Chemistry 2013, 85 (18), 8498-8502.
- 10. Aliyari, E.; Konermann, L., Formation of Gaseous Peptide Ions from Electrospray Droplets: Competition between the Ion Evaporation Mechanism and Charged Residue Mechanism. Analytical Chemistry 2022, 94 (21), 7713-7721.
- 11. Novotny, M., New detection strategies through supercritical fluid chromatography. Journal of High Resolution Chromatography 1986, 9 (3), 137-144.
- 12. Haglind, A.; Hedeland, M.; Arvidsson, T.; Pettersson, C. E., Major signal suppression from metal ion clusters in SFC/ESI-MS Cause and effects. Journal of Chromatography B 2018, 1084, 96-105.
- 13. Mostafa, M. E.; Grinias, J. P.; Edwards, J. L., Supercritical Fluid Nanospray Mass Spectrometry. Journal of the American Society for Mass Spectrometry 2022.
- 14. Fenn, J. B., Ion formation from charged droplets: Roles of geometry, energy, and time. Journal of the American Society for Mass Spectrometry 1993, 4 (7), 524-535.
- 15. Cech, N. B.; Enke, C. G., Selectivity in Electrospray Ionization Mass Spectrometry. Electrospray and MALDI Mass Spectrometry 2010, 49-73.

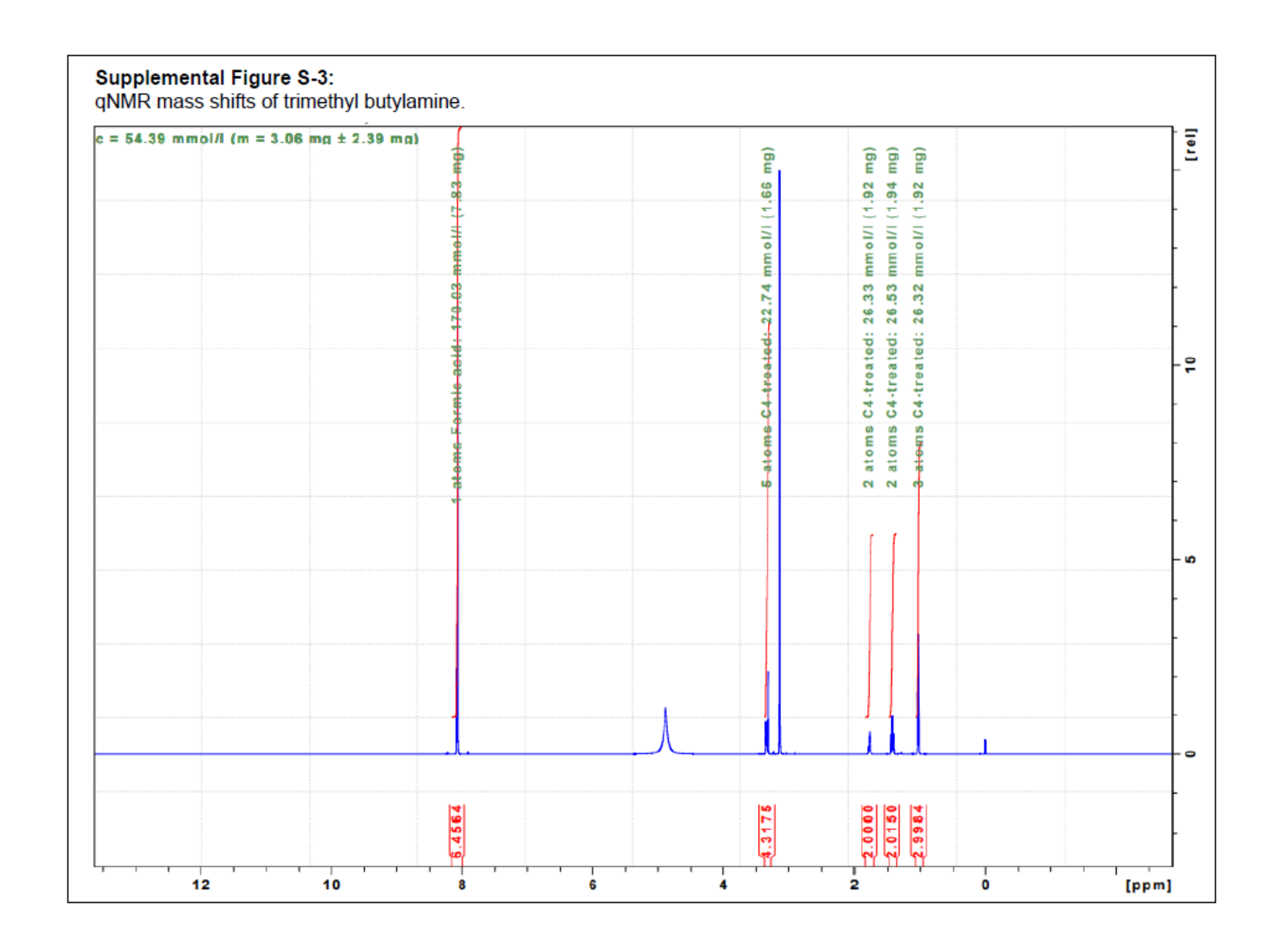
- 16. Enke, C. G., A Predictive Model for Matrix and Analyte Effects in Electrospray Ionization of Singly-Charged Ionic Analytes. Analytical Chemistry 1997, 69 (23), 4885-4893.
- 17. Tang, K.; Page, J. S.; Smith, R. D., Charge competition and the linear dynamic range of detection in electrospray ionization mass spectrometry. Journal of the American Society for Mass Spectrometry 2004, 15 (10), 1416-1423.
- 18. Sindelar, M.; Patti, G. J., Chemical Discovery in the Era of Metabolomics. Journal of the American Chemical Society 2020, 142 (20), 9097-9105.
- 19. Gass, D. T.; Quintero, A. V.; Hatvany, J. B.; Gallagher, E. S., Metal adduction in mass spectrometric analyses of carbohydrates and glycoconjugates. Mass Spectrometry Reviews 2022, n/a (n/a), e21801.
- 20. Mostafa, M. E.; Grinias, J. P.; Edwards, J. L., Evaluation of Nanospray Capillary LC-MS Performance for Metabolomic Analysis in Complex Biological Matrices. Journal of Chromatography A 2022, 462952.
- 21. Edwards, J. L.; Edwards, R. L.; Reid, K. R.; Kennedy, R. T., Effect of decreasing column inner diameter and use of off-line two-dimensional chromatography on metabolite detection in complex mixtures. Journal of Chromatography A 2007, 1172 (2), 127-134.
- 22. Haskins, W. E.; Wang, Z.; Watson, C. J.; Rostand, R. R.; Witowski, S. R.; Powell, D. H.; Kennedy, R. T., Capillary LC–MS2 at the Attomole Level for Monitoring and Discovering Endogenous Peptides in Microdialysis Samples Collected in Vivo. Analytical Chemistry 2001, 73 (21), 5005-5014.
- 23. Schneider, C. A.; Rasband, W. S.; Eliceiri, K. W., NIH Image to ImageJ: 25 years of image analysis. Nature Methods 2012, 9 (7), 671-675.
- 24. Dewald, H. D., Electrospray Ionization Mass Spectrometry: Fundamentals, Instrumentation and Applications (ed. Cole, Richard B.). Journal of Chemical Education 1999, 76 (1), 33.
- 25. Lentz, N.; Houk, R., Negative ion mode electrospray ionization mass spectrometry study of ammonium-counter ion clusters. Journal of the American Society for Mass Spectrometry 2007, 18, 285-293.
- 26. Racine, J. S., RSTUDIO: A PLATFORM-INDEPENDENT IDE FOR R AND SWEAVE. Journal of Applied Econometrics 2012, 27 (1), 167-172.
- 27. Guan, S.; Rabus, J. M.; Maître, P.; Bythell, B. J., Gas-Phase Dissociation Chemistry of Deprotonated RGD. Journal of the American Society for Mass Spectrometry 2020, 32 (1), 55-63.
- 28. Marianski, M.; Supady, A.; Ingram, T.; Schneider, M.; Baldauf, C., Assessing the accuracy of across-the-scale methods for predicting carbohydrate conformational energies for the examples of glucose and α -maltose. Journal of chemical theory and computation 2016, 12 (12), 6157-6168.
- 29. Supady, A.; Blum, V.; Baldauf, C., First-principles molecular structure search with a genetic algorithm. Journal of Chemical Information and Modeling 2015, 55 (11), 2338-2348.
- 30. and, G. L.; and, P. T.; and, B. K.; and, R.; and, s.; and, g.; and, R. V.; and, N.; and, E. K.; and, D. C.; and, A. D.; and, D. N.; and, G. J.; and, B. C.; and, M. S.; and, S. T.; and, A.; and, A. V.; and, M. W.; and, I. T.; and, D. P.; and, K. U.; and, V. F. S.; and, g. g.; and, A. P.; and, F. B.; and, J.; and, s.; and, J.; DoliathGavid rdkit/rdkit: 2022_03_5 (Q1 2022) Release. https://doi.org/10.5281/zenodo.6961488.
- 31. Halgren, T. A., Merck molecular force field. I. Basis, form, scope, parameterization, and performance of MMFF94. Journal of computational chemistry 1996, 17 (5-6), 490-519.
- 32. Zhao, Y.; Truhlar, D. G., The M06 suite of density functionals for main group thermochemistry, thermochemical kinetics, noncovalent interactions, excited states, and transition elements: two new functionals and systematic testing of four M06-class functionals and 12 other functionals. Theoretical Chemistry Accounts 2008, 120 (1), 215-241.
- 33. Morrison, K. A.; Bythell, B. J.; Clowers, B. H., Interrogating Proton Affinities of Organophosphonate Species Via Atmospheric Flow Tube Mass Spectrometry and Computational Methods. Journal

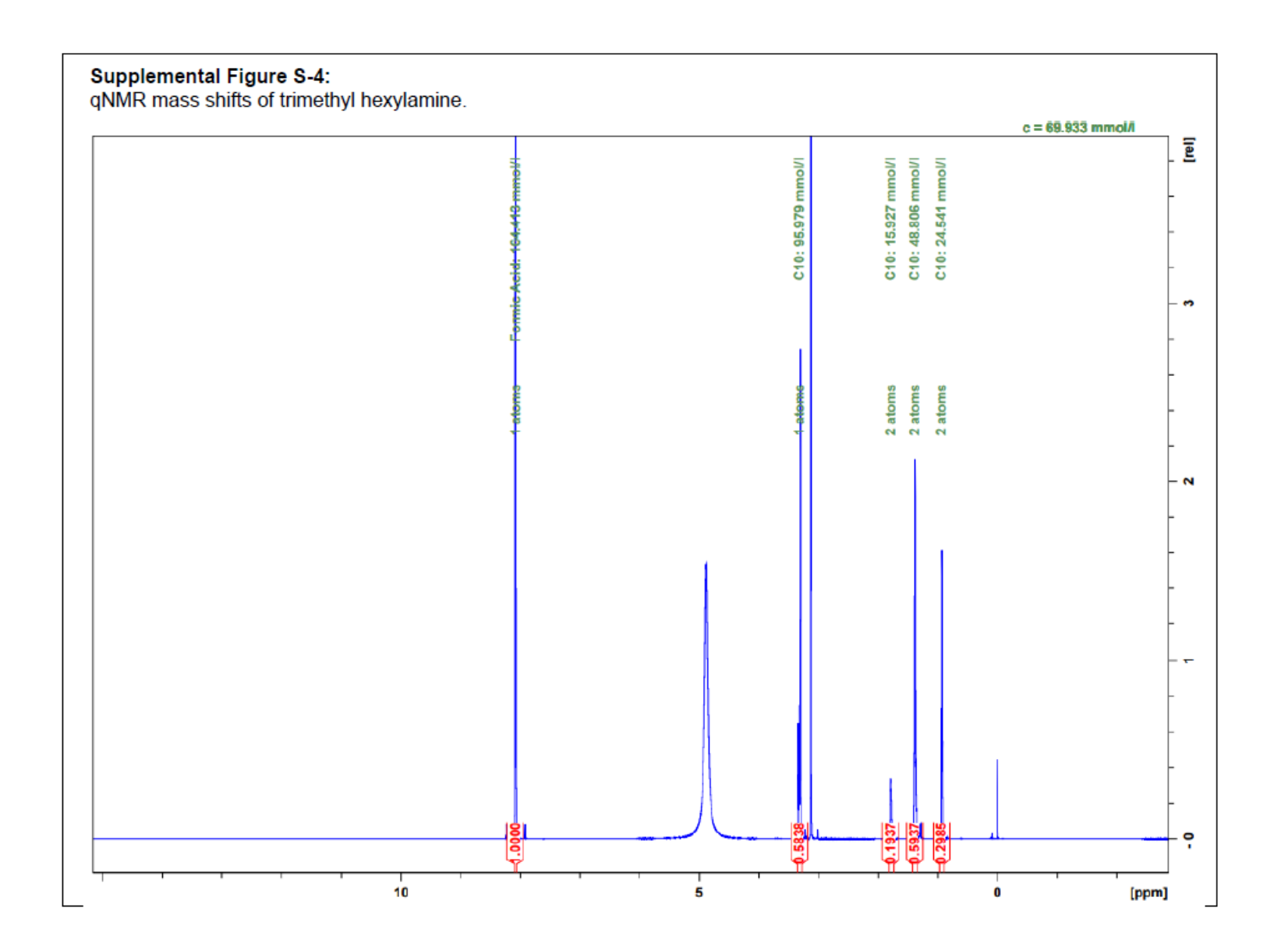
- of The American Society for Mass Spectrometry 2019, 30 (7), 1308-1320.
- 34. Said, R. B.; Kolle, J. M.; Essalah, K.; Tangour, B.; Sayari, A., A Unified Approach to CO2–Amine Reaction Mechanisms. ACS Omega 2020, 5 (40), 26125-26133.
- 35. Fischer, H.; Gyllenhaal, O.; Vessman, J.; Albert, K., Reaction Monitoring of Aliphatic Amines in Supercritical Carbon Dioxide by Proton Nuclear Magnetic Resonance Spectroscopy and Implications for Supercritical Fluid Chromatography. Analytical Chemistry 2003, 75 (3), 622-626.
- 36. Berger, T. A., Effect of density on kinetic performance in supercritical fluid chromatography with methanol modified carbon dioxide. Journal of Chromatography A 2018, 1564, 188-198.
- 37. West, C.; Melin, J.; Ansouri, H.; Mengue Metogo, M., Unravelling the effects of mobile phase additives in supercritical fluid chromatography. Part I: Polarity and acidity of the mobile phase. Journal of Chromatography A 2017, 1492, 136-143.
- 38. Berger, T. A., Characterization of a 2.6µm Kinetex porous shell hydrophilic interaction liquid chromatography column in supercritical fluid chromatography with a comparison to 3µm totally porous silica. Journal of Chromatography A 2011, 1218 (28), 4559-4568.
- 39. Phinney, K. W.; Sander, L. C., Additive concentration effects on enantioselective separations in supercritical fluid chromatography. Chirality 2003, 15 (4), 287-294.
- 40. Liigand, J.; Laaniste, A.; Kruve, A., pH Effects on Electrospray Ionization Efficiency. Journal of The American Society for Mass Spectrometry 2017, 28 (3), 461-469.
- 41. Shackman, H. M.; Ding, W.; Bolgar, M. S., A Novel Route to Recognizing Quaternary Ammonium Cations Using Electrospray Mass Spectrometry. Journal of the American Society for Mass Spectrometry 2015, 26 (1), 181-189.
- 42. Raffaelli, A.; Bruins, A. P., Factors affecting the ionization efficiency of quaternary ammonium compounds in electrospray/ionspray mass spectrometry. Rapid Communications in Mass Spectrometry 1991, 5 (6), 269-275.
- 43. Cazenave-Gassiot, A.; Boughtflower, R.; Caldwell, J.; Hitzel, L.; Holyoak, C.; Lane, S.; Oakley, P.; Pullen, F.; Richardson, S.; Langley, G. J., Effect of increasing concentration of ammonium acetate as an additive in supercritical fluid chromatography using CO2–methanol mobile phase. Journal of Chromatography A 2009, 1216 (36), 6441-6450.
- 44. Roy, D.; Wahab, M. F.; Berger, T. A.; Armstrong, D. W., Ramifications and Insights on the Role of Water in Chiral Sub/Supercritical Fluid Chromatography. Analytical Chemistry 2019, 91 (22), 14672-14680.
- 45. Cech, N. B.; Enke, C. G., Relating Electrospray Ionization Response to Nonpolar Character of Small Peptides. Analytical Chemistry 2000, 72 (13), 2717-2723.
- 46. Raabe, G.; Wang, Y.; Fleischhauer, J., Calculation of the Proton Affinities of Primary, Secondary, and Tertiary Amines Using Semiempirical and ab initio Methods. 2000, 55 (8), 687-694.
- 47. Urban, P. L., Clarifying Misconceptions about Mass and Concentration Sensitivity. Journal of Chemical Education 2016, 93 (6), 984-987.
- 48. Tarafder, A., Designs and methods for interfacing SFC with MS. Journal of Chromatography B 2018, 1091, 1-13.
- 49. Akbal, L.; Hopfgartner, G., Effects of liquid post-column addition in electrospray ionization performance in supercritical fluid chromatography—mass spectrometry. Journal of Chromatography A 2017, 1517, 176-184.
- 50. Tarafder, A.; Guiochon, G., Extended zones of operations in supercritical fluid chromatography. Journal of Chromatography A 2012, 1265, 165-175.
- 51. Jordan, J. S.; Williams, E. R., Effects of Electrospray Droplet Size on Analyte Aggregation: Evidence for Serine Octamer in Solution. Analytical Chemistry 2021, 93 (3), 1725-1731.
- 52. Jordan, J. S.; Xia, Z.; Williams, E. R., Tips on Making Tiny Tips: Secrets to Submicron Nanoelectrospray Emitters. Journal of the American Society for Mass Spectrometry 2022, 33 (3), 607-611.

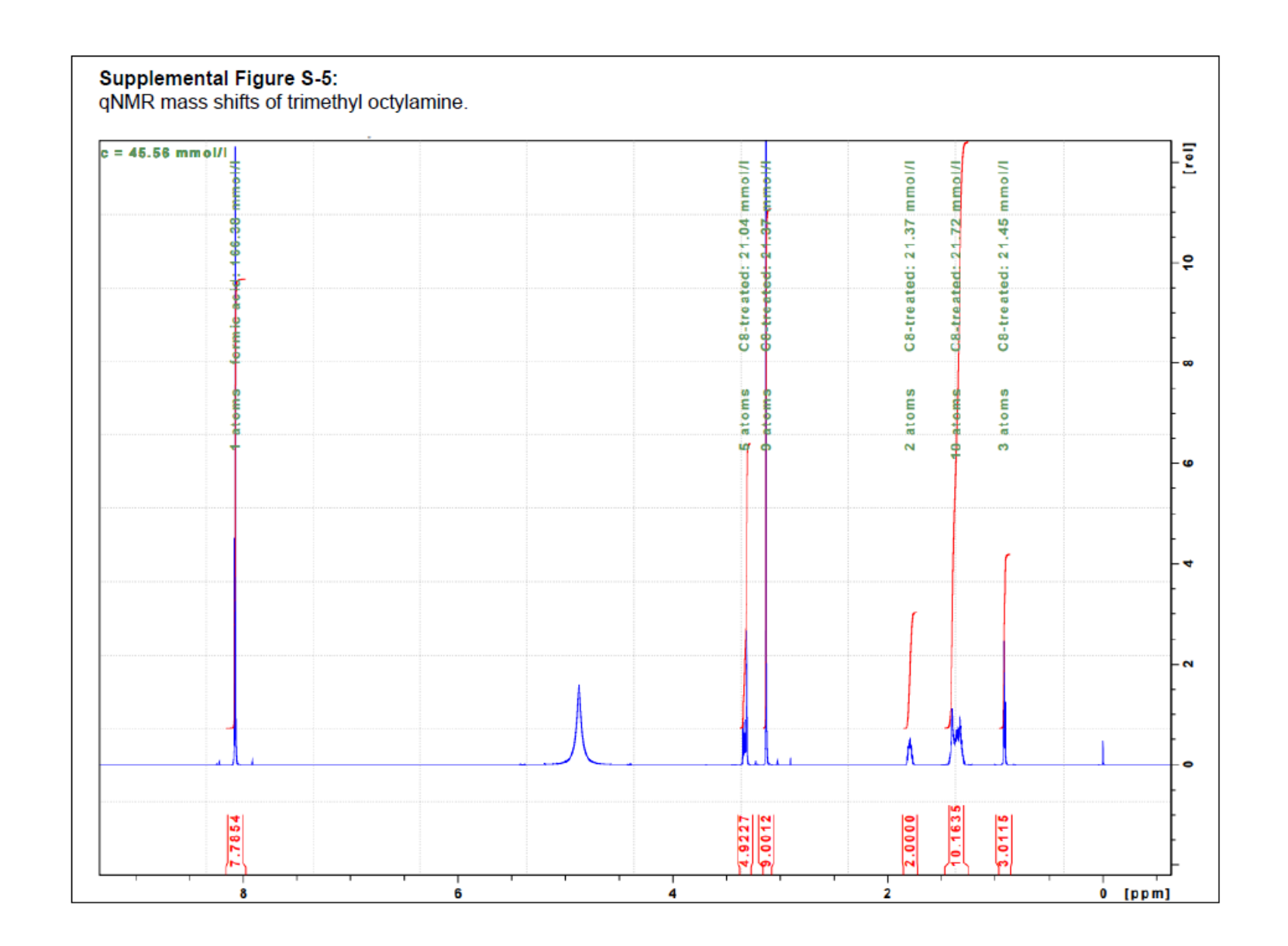
- 53. Aue, D. H.; Webb, H. M.; Bowers, M. T., Quantitative proton affinities, ionization potentials, and hydrogen affinities of alkylamines. Journal of the American Chemical Society 1976, 98 (2), 311-317.
- 54. Gaskell, S. J., Electrospray: principles and practice. Journal of mass spectrometry 1997, 32 (7), 677-688.
- 55. Znamenskiy, V.; Marginean, I.; Vertes, A., Solvated Ion Evaporation from Charged Water Nanodroplets. The Journal of Physical Chemistry A 2003, 107 (38), 7406-7412.
- 56. Liu, C. C.; Zhang, J.; Dovichi, N. J., A sheath-flow nanospray interface for capillary electrophoresis/mass spectrometry. Rapid Communications in Mass Spectrometry 2005, 19 (2), 187-192.
- 57. Hunter, E. P. L.; Lias, S. G., Evaluated Gas Phase Basicities and Proton Affinities of Molecules: An Update. Journal of Physical and Chemical Reference Data 1998, 27 (3), 413-656.
- 58. Umeyama, H.; Morokuma, K., Origin of alkyl substituent effect in the proton affinity of amines, alcohols, and ethers. Journal of the American Chemical Society 1976, 98 (15), 4400-4404.
- 59. Fenn, J. B.; Mann, M.; Meng, C. K.; Wong, S. F.; Whitehouse, C. M., Electrospray ionization–principles and practice. Mass Spectrometry Reviews 1990, 9 (1), 37-70.
- 60. El-Faramawy, A.; Siu, K. W. M.; Thomson, B. A., Efficiency of nano-electrospray ionization. Journal of the American Society for Mass Spectrometry 2005, 16 (10), 1702-1707.
- 61. Cox, J. T.; Marginean, I.; Smith, R. D.; Tang, K., On the ionization and ion transmission efficiencies of different ESI-MS interfaces. Journal of the American Society for Mass Spectrometry 2015, 26 (1), 55-62.
- 62. Kelley, M. P.; Davis, A.; Clowers, B.; Clark, A. E.; Clark, S. B., Acceleration of metal–ligand complexation kinetics by electrospray ionization. Analyst 2017, 142 (23), 4468-4475.
- 63. Schug, K.; McNair, H. M., Adduct formation in electrospray ionization mass spectrometry: II. Benzoic acid derivatives. Journal of Chromatography A 2003, 985 (1), 531-539.
- 64. Calixte, E. I.; Liyanage, O. T.; Gass, D. T.; Gallagher, E. S., Formation of Carbohydrate–Metal Adducts from Solvent Mixtures during Electrospray: A Molecular Dynamics and ESI-MS Study. Journal of the American Society for Mass Spectrometry 2021, 32 (12), 2738-2745.
- 65. Kaplitz, A. S.; Mostafa, M. E.; Calvez, S. A.; Edwards, J. L.; Grinias, J. P., Two-dimensional separation techniques using supercritical fluid chromatography. Journal of Separation Science 2021, 44 (1), 426-437.
- 66. Bennett, R.; Olesik, S. V., Enhanced fluidity liquid chromatography of inulin fructans using ternary solvent strength and selectivity gradients. Analytica Chimica Acta 2018, 999, 161-168.
- 67. van de Velde, B.; Guillarme, D.; Kohler, I., Supercritical fluid chromatography Mass spectrometry in metabolomics: Past, present, and future perspectives. Journal of Chromatography B 2020, 1161, 122444.

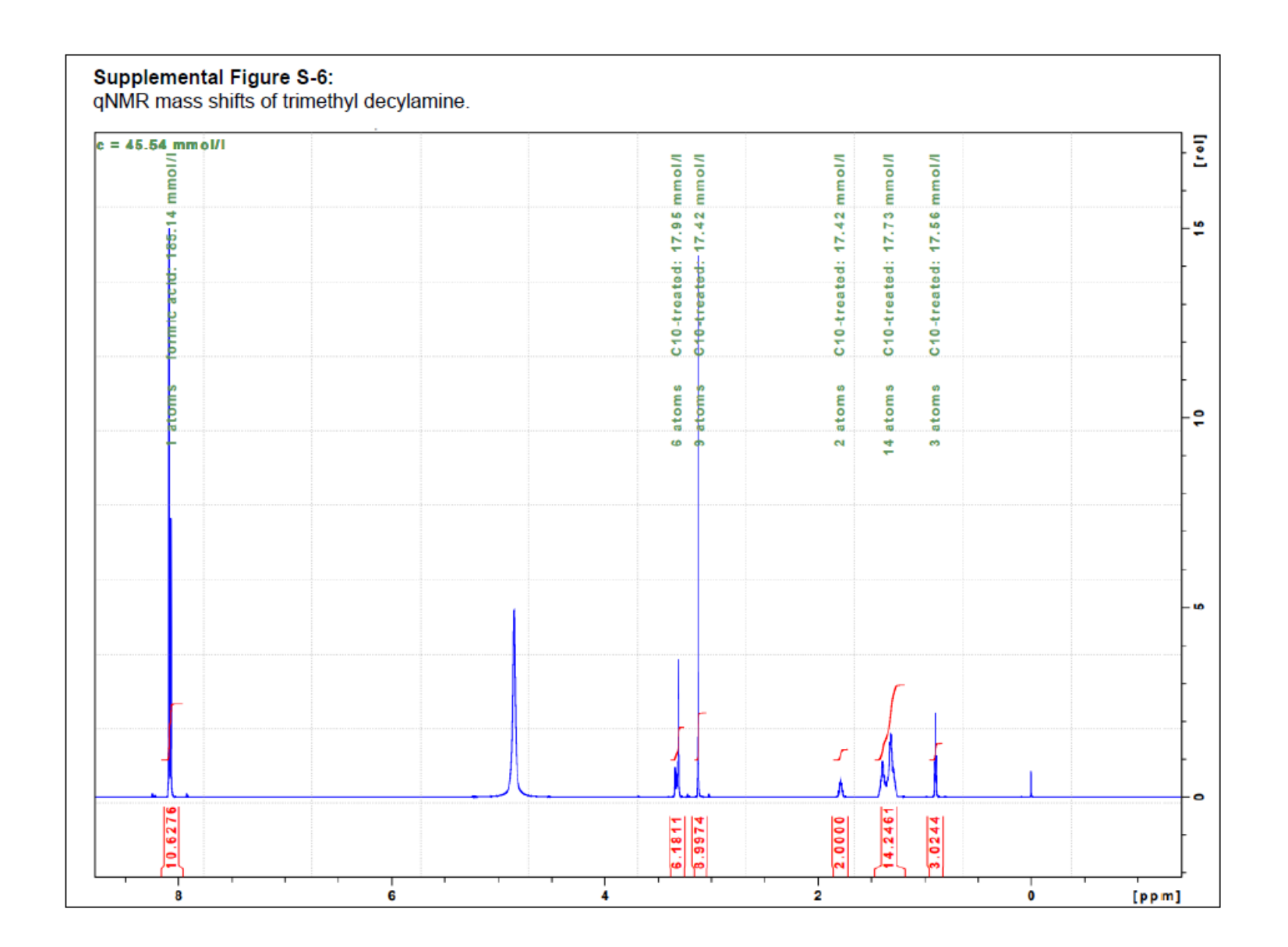




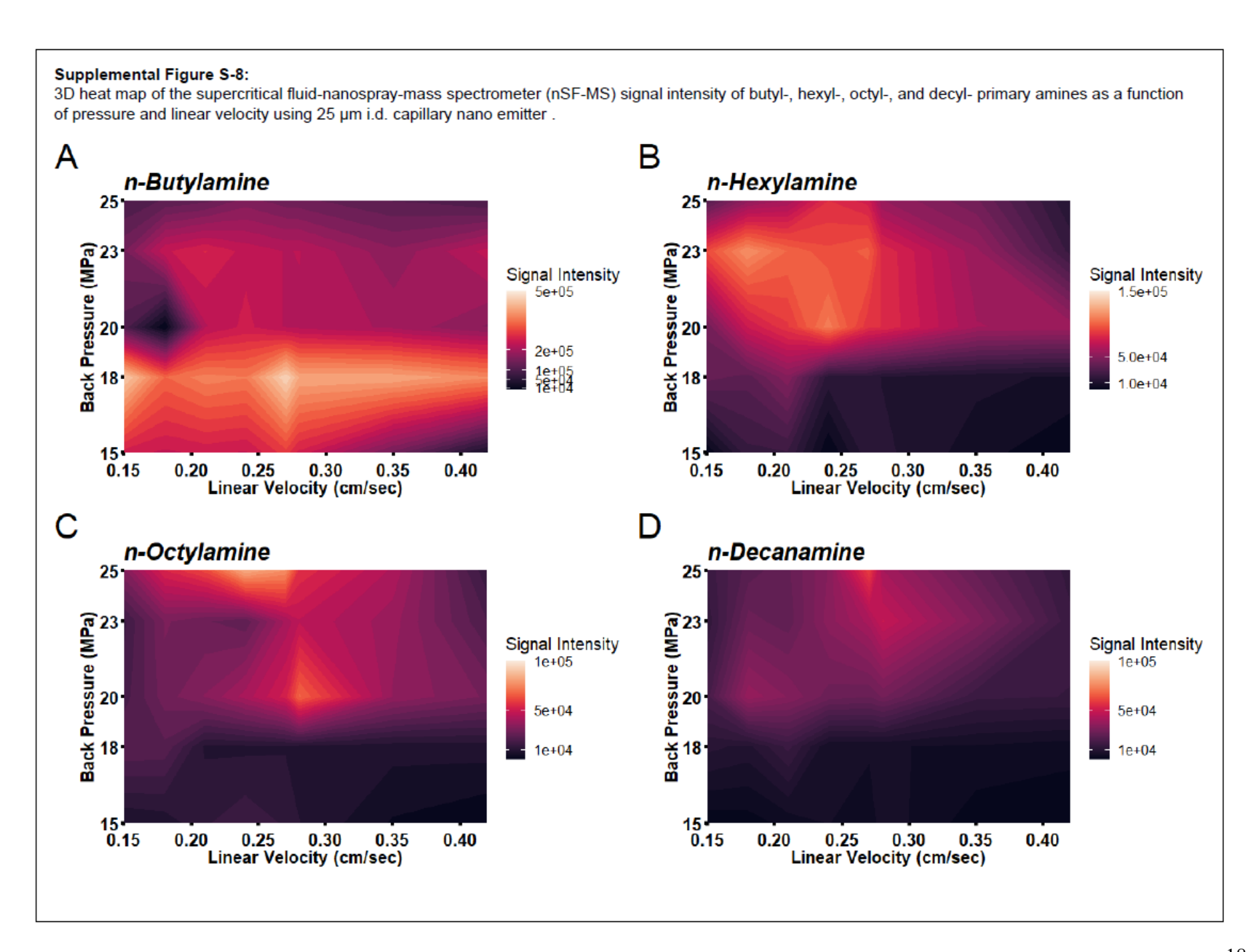


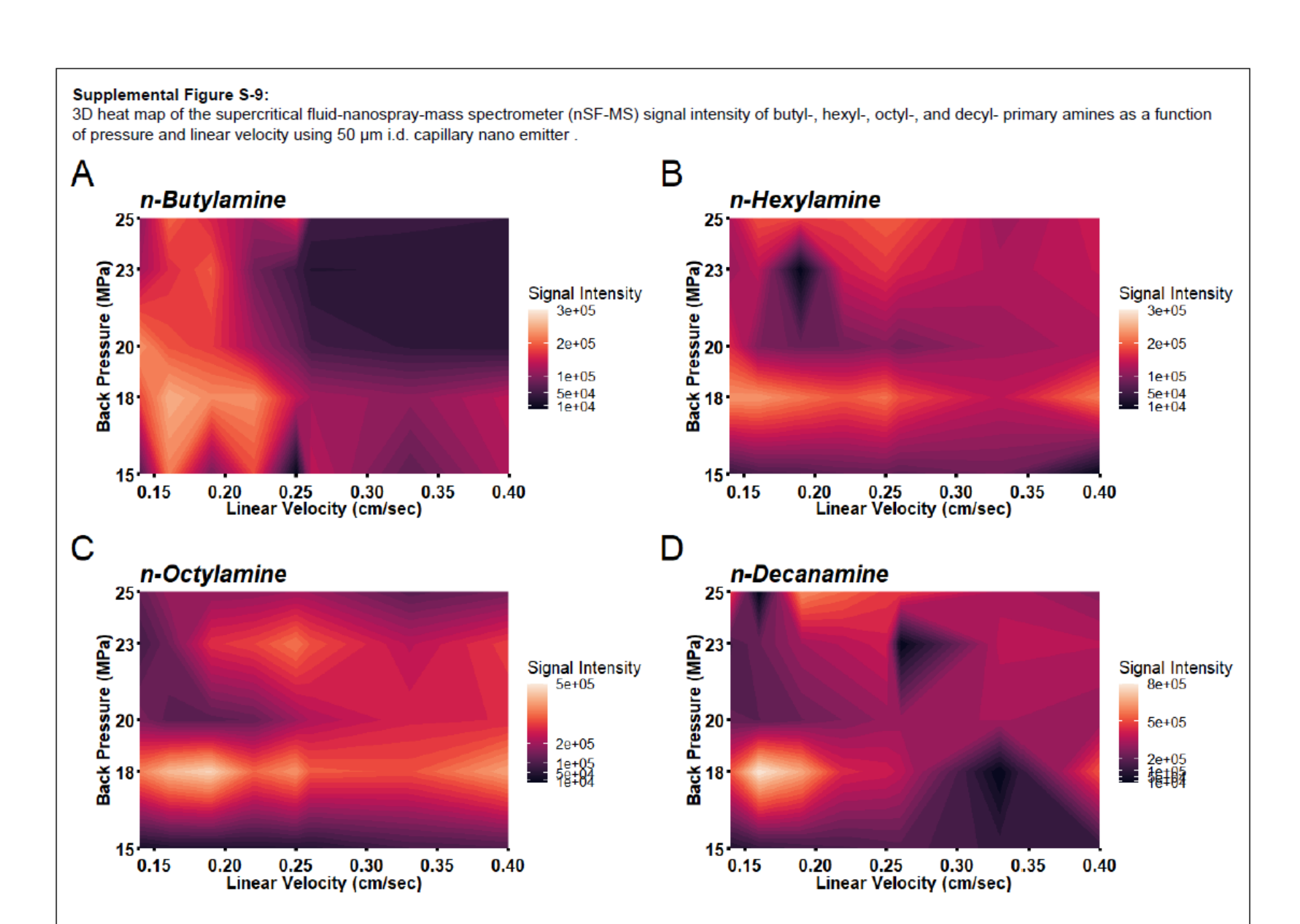






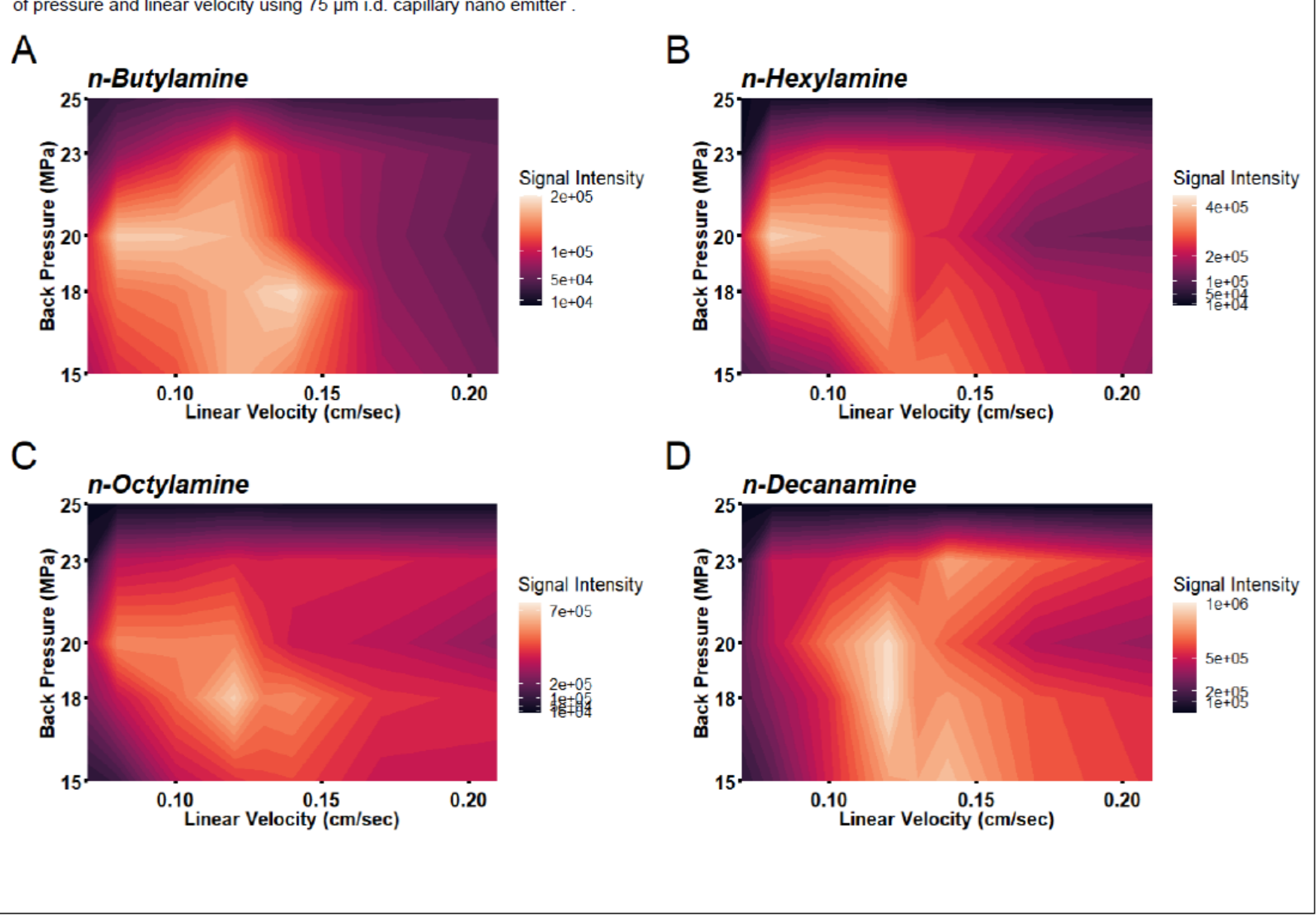
Supplemental Figure \$-7: LIT-MS spectrum of a separate injections of A) primary hexylamine B) secondary hexylamine standards showing the absence of amines reaction with sCO₂ contaminants. A 1 μL injection of 50 μM standard was injected at 18 MPa, at 50 °C using 90 % sCO₂ with 10 % methanol (0.01 % formic acid final concentration) nano-emitted by the 75 µm tip at 0.14 cm/sec. A Signal: 6.37E5 100 95 102.13 90 85 80 75 Relative Abundance 146.12 25 20 15 10 5 103.68 106 108 110 112 114 116 118 120 122 124 126 128 130 132 134 136 138 140 142 144 146 148 150 m/z **B** Signal: 1.73E6 100 116.22 95 90 85 80 🖥 75 Relative Abundance 160.13 30 🖥 ŅΘ 25 🖥 20 15 10 5 117.17 116 118 120 122 124 126 128 130 132 134 136 138 140 142 144 146 148 150 152 154 156 158 160 162 164 m/z





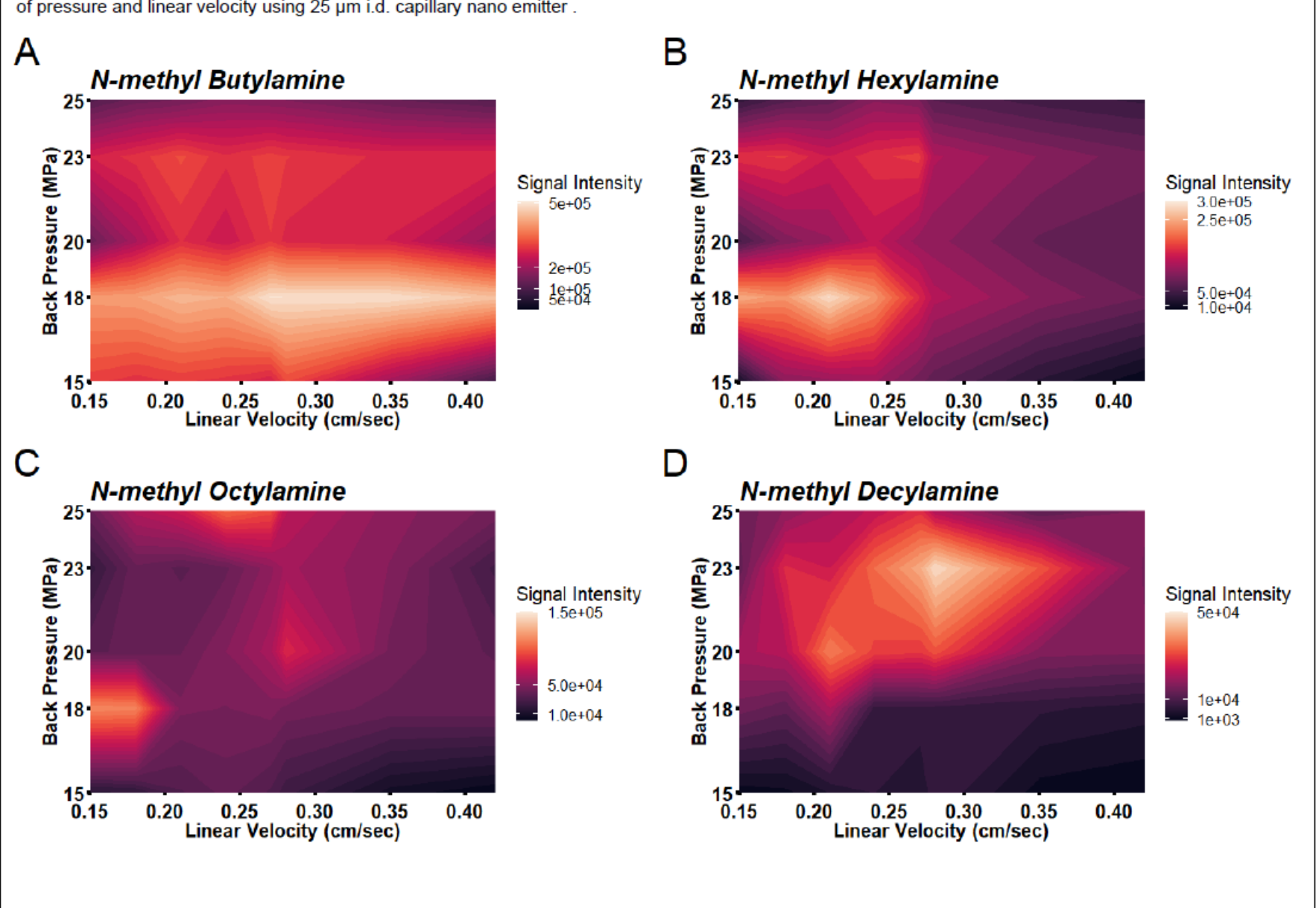
Supplemental Figure S-10:

3D heat map of the supercritical fluid-nanospray-mass spectrometer (nSF-MS) signal intensity of butyl-, hexyl-, octyl-, and decyl- primary amines as a function of pressure and linear velocity using 75 µm i.d. capillary nano emitter .



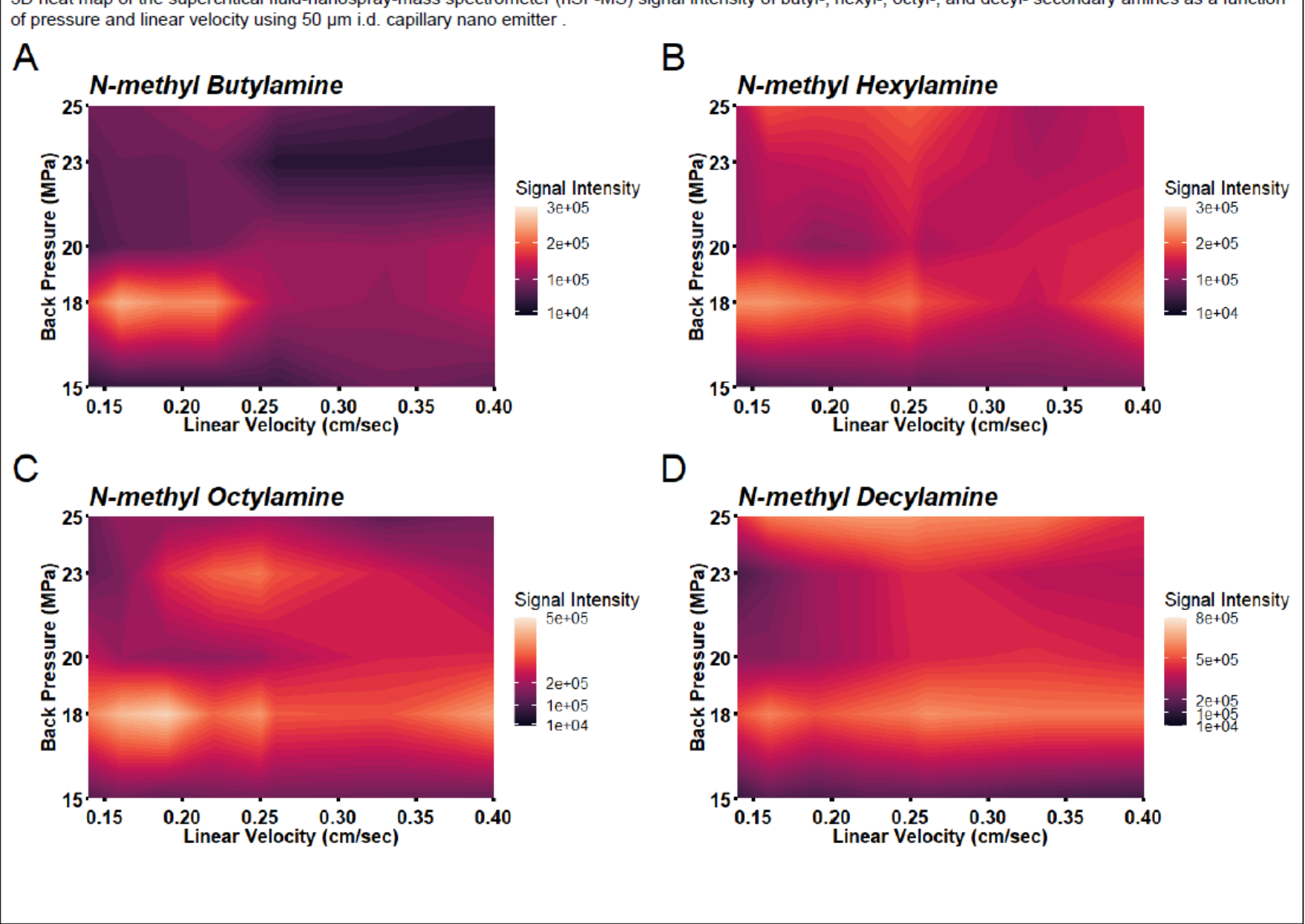
Supplemental Figure S-11:

3D heat map of the supercritical fluid-nanospray-mass spectrometer (nSF-MS) signal intensity of butyl-, hexyl-, octyl-, and decyl- secondary amines as a function of pressure and linear velocity using 25 µm i.d. capillary nano emitter .



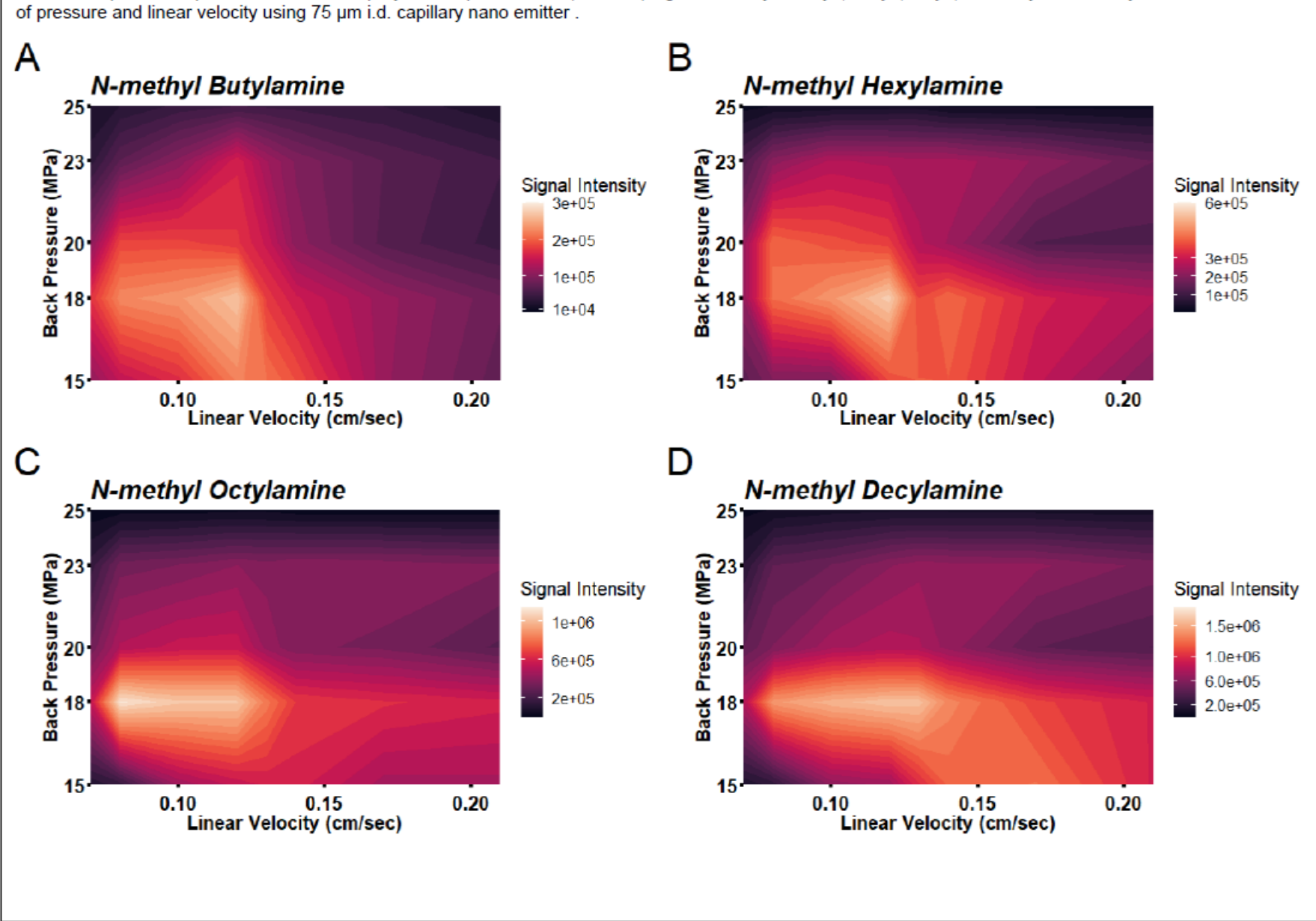


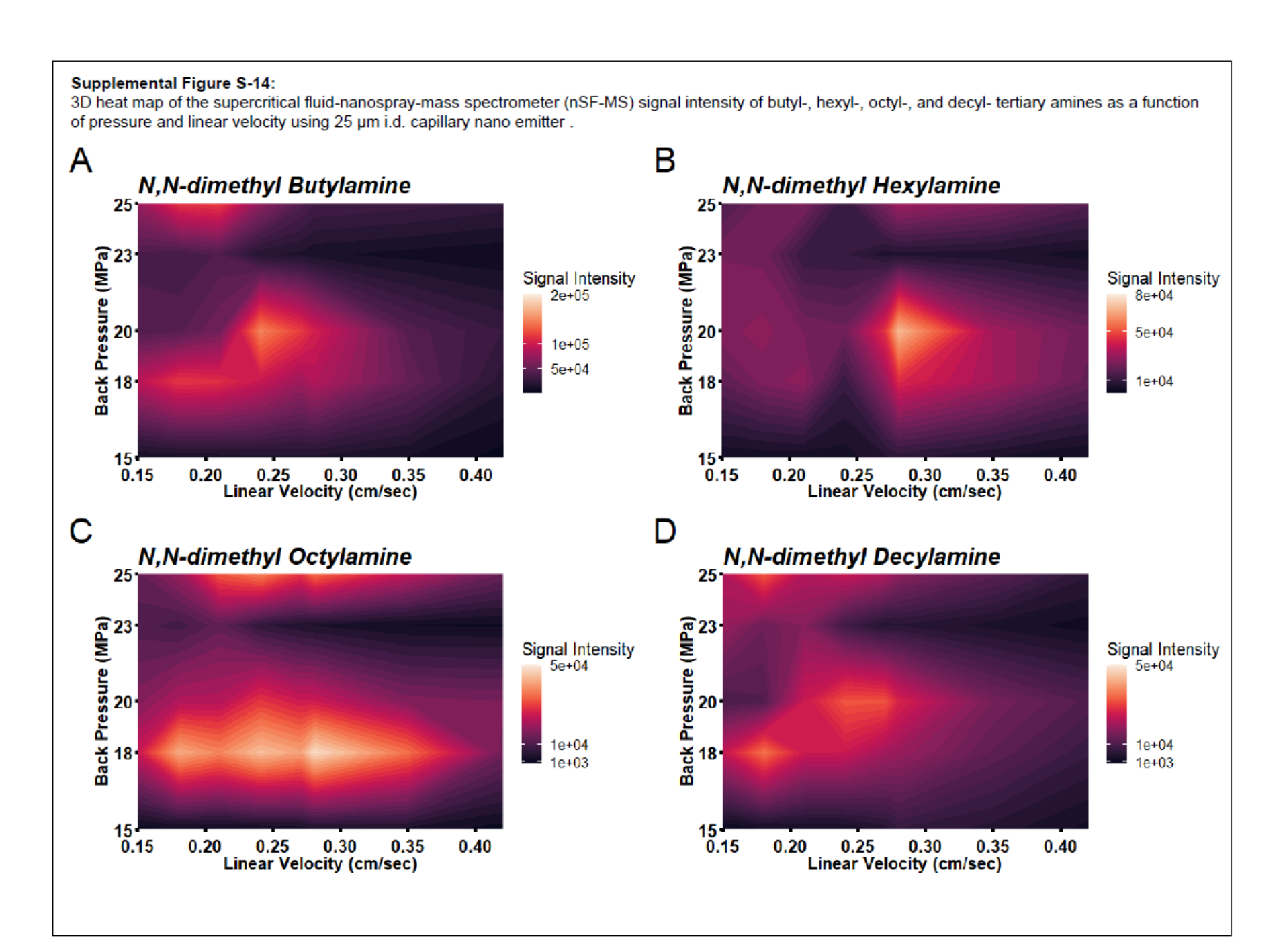
3D heat map of the supercritical fluid-nanospray-mass spectrometer (nSF-MS) signal intensity of butyl-, hexyl-, octyl-, and decyl- secondary amines as a function of pressure and linear velocity using 50 µm i.d. capillary nano emitter .

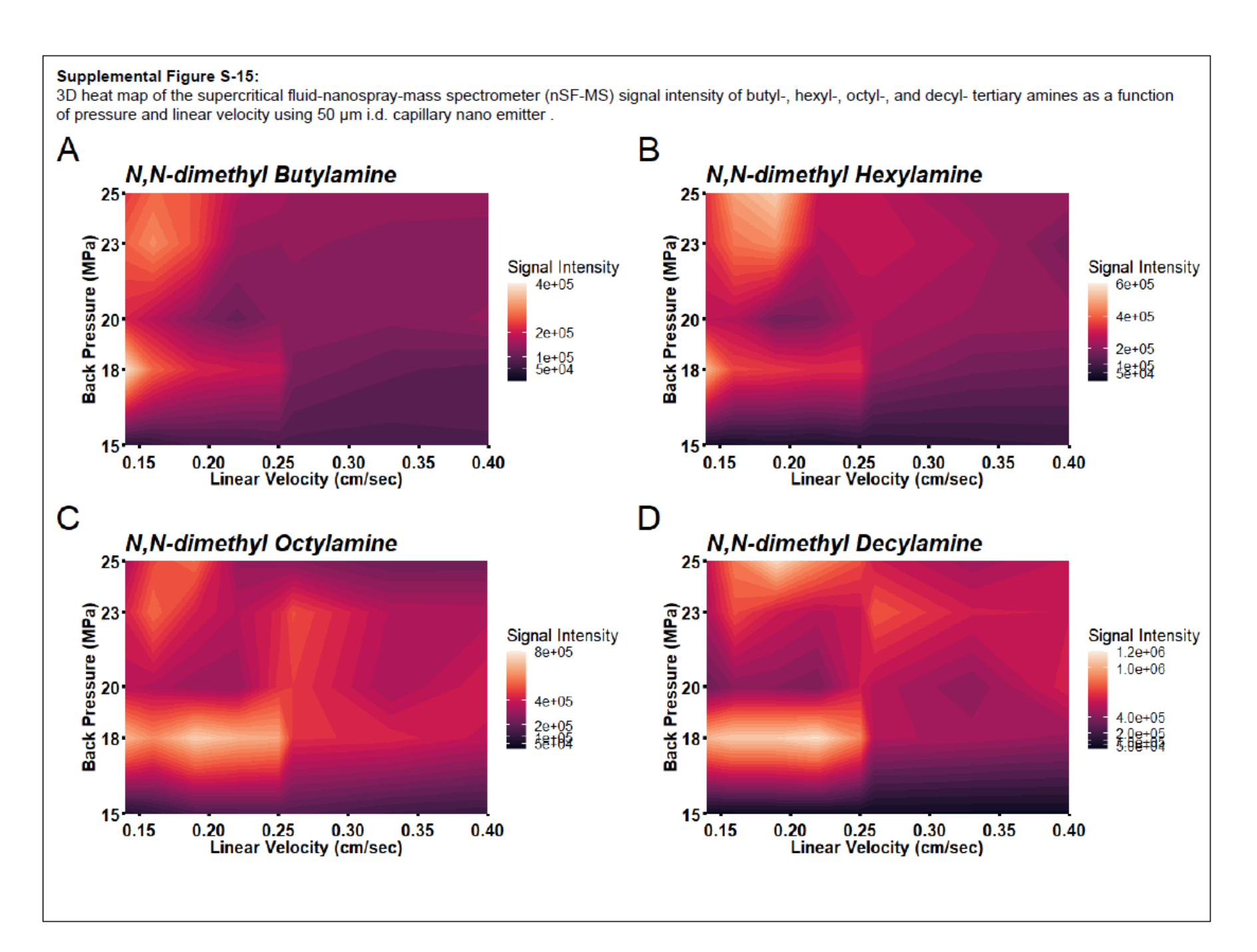


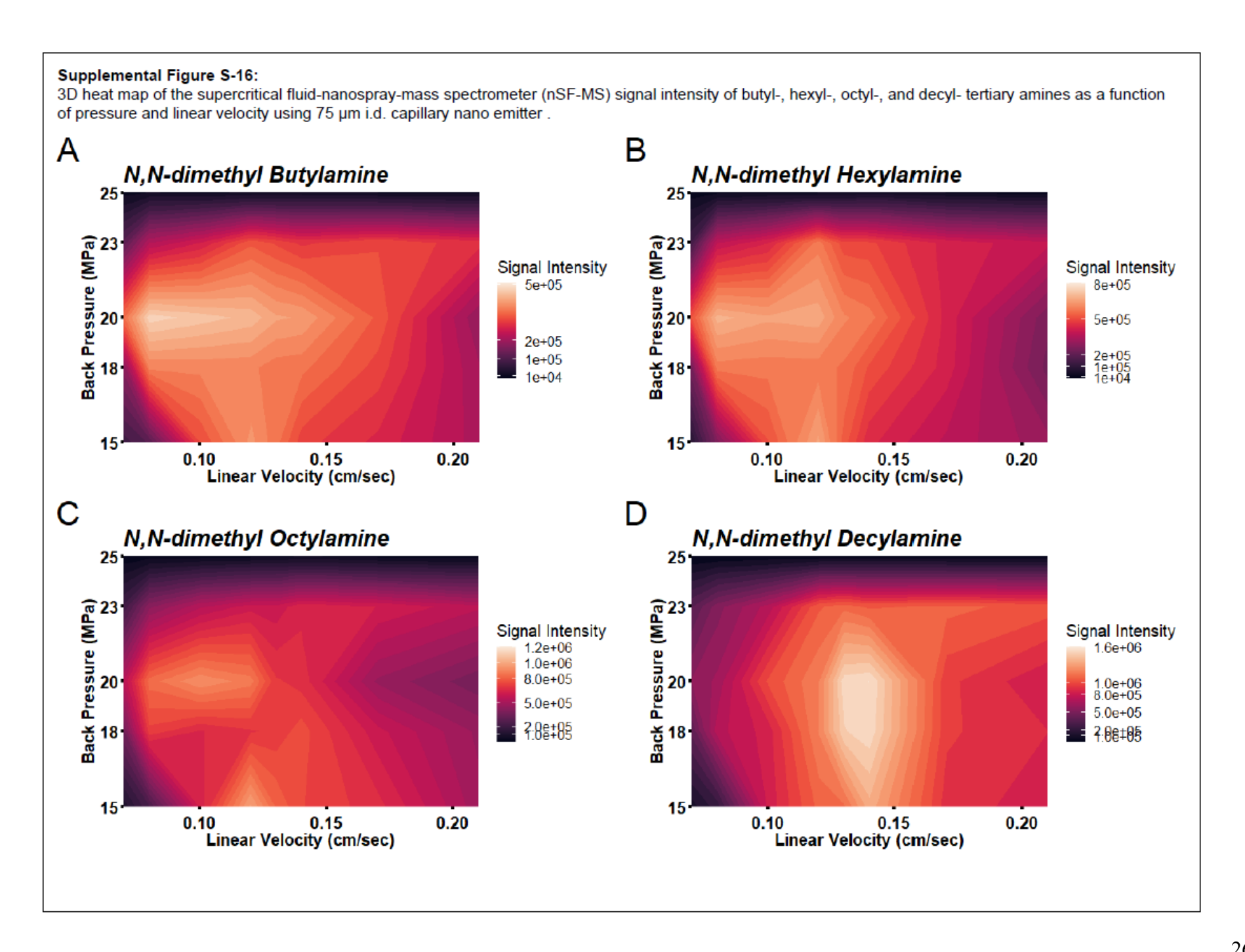


3D heat map of the supercritical fluid-nanospray-mass spectrometer (nSF-MS) signal intensity of butyl-, hexyl-, octyl-, and decyl- secondary amines as a function of pressure and linear velocity using 75 µm i.d. capillary nano emitter .



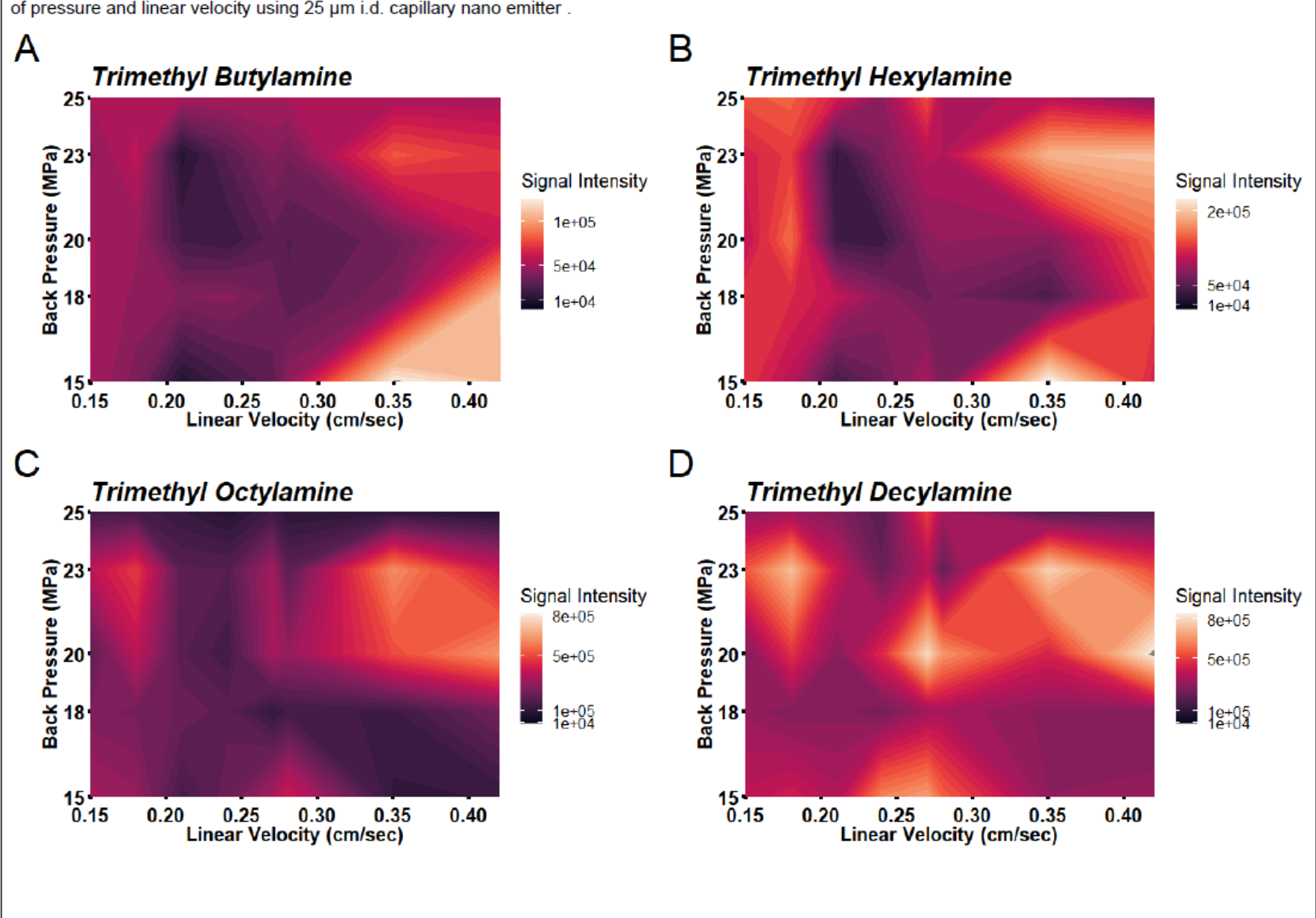


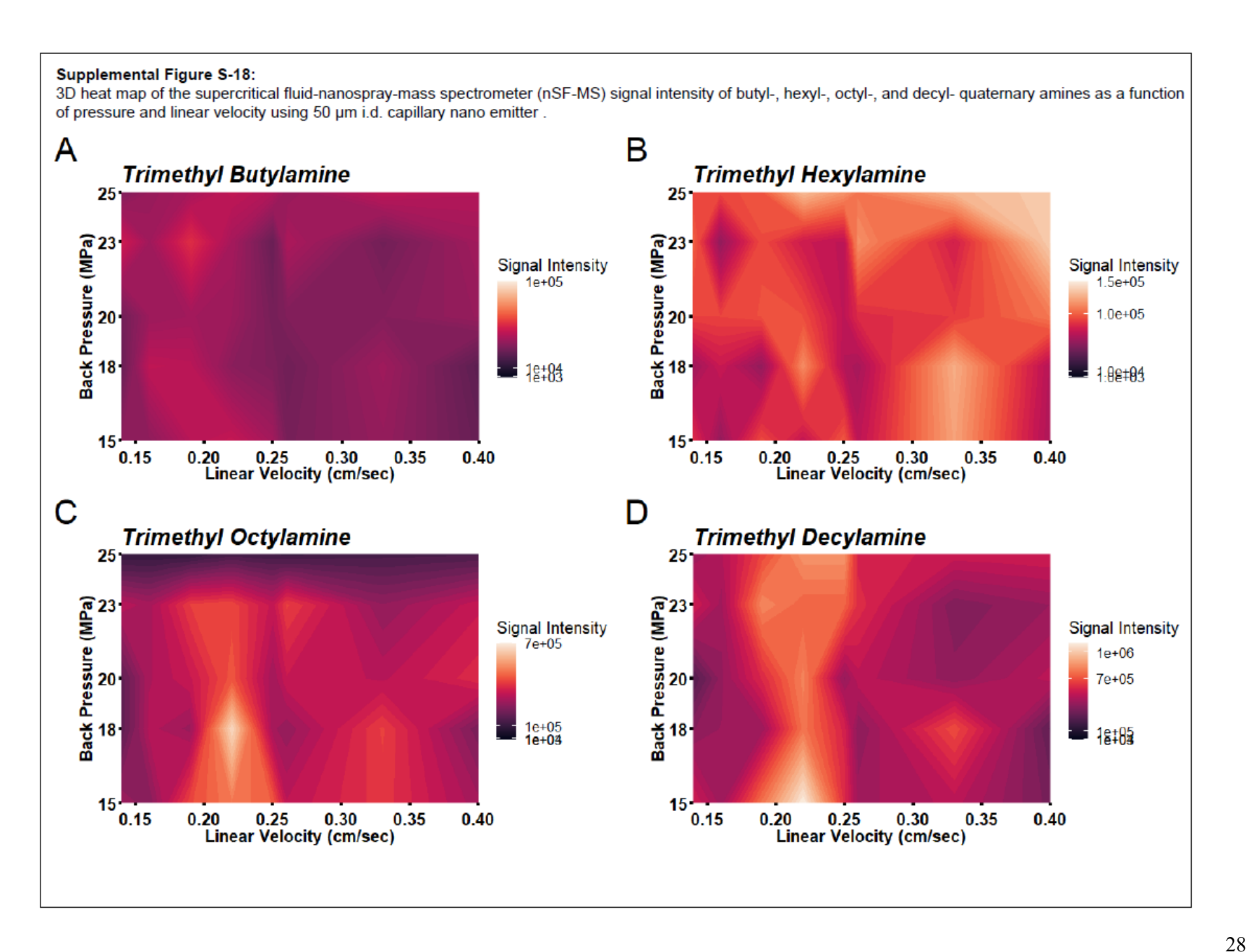




Supplemental Figure S-17:

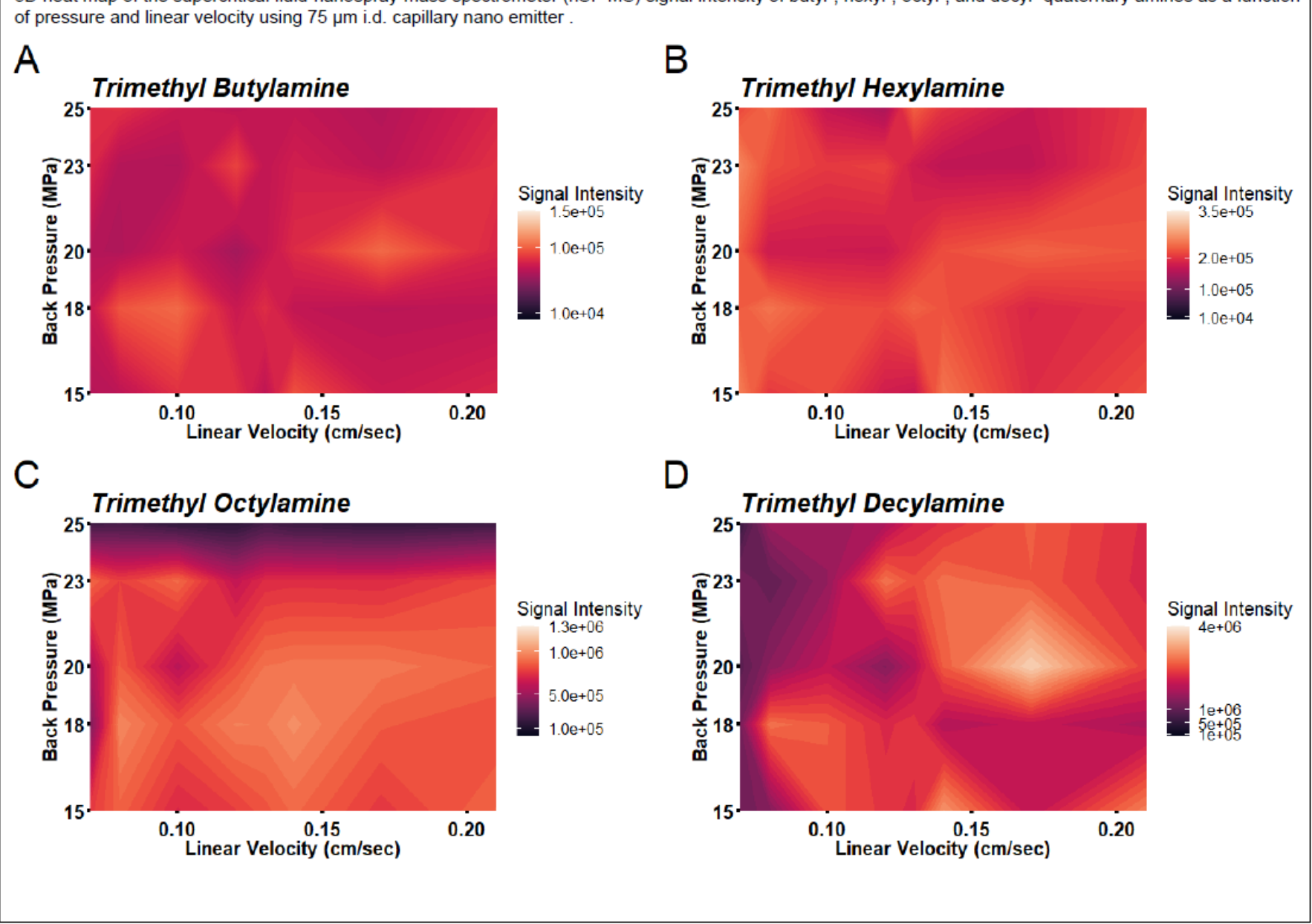
3D heat map of the supercritical fluid-nanospray-mass spectrometer (nSF-MS) signal intensity of butyl-, hexyl-, octyl-, and decyl- quaternary amines as a function of pressure and linear velocity using 25 µm i.d. capillary nano emitter .





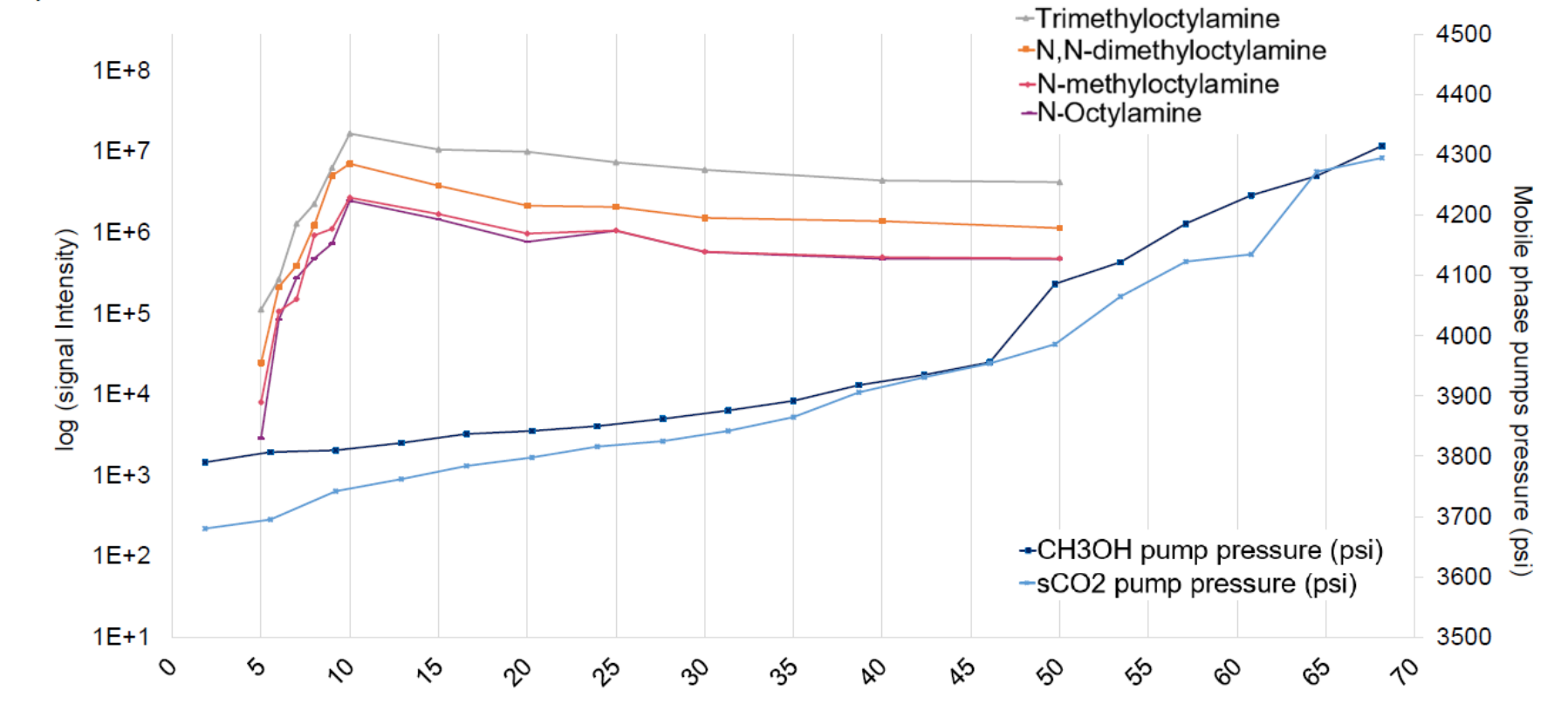
Supplemental Figure S-19:

3D heat map of the supercritical fluid-nanospray-mass spectrometer (nSF-MS) signal intensity of butyl-, hexyl-, octyl-, and decyl- quaternary amines as a function



Supplemental Figure S-20:

The effect of changing modifier percentage %CH₃OH on mobile phase pumps pressure and signal intensity. The change of C₈ primary, secondary, tertiary, and quaternary amines signal effect on nSF-MS at 50 °C, 18MPa, 1.0mL/min sCO₂ using 75 μm i.d. capillary interface. Nanospraying less than 5 % methanol in sCO₂ gave no MS signal. Increasing the methanol percentage from 5 – 10 % showed a signal intensity increase for all the amines classes. A slight signal intensity drop was found after 10 % methanol. This may be explained by the drastic change in density with the liquid modifier % increase in the sCO₂.38 A linear CO₂ and CH₃OH pump pressure increase was found using 5 - 40 % methanol whereas an exponentially increasing trend was found above 40 %. Exceeding the modifier above 50 – 66 %, depending on the flow rate, was followed by a density error.³⁸ The excessive pressure difference found between the pumps and the BPR along with the density error may indicate the SF state loss.³⁹



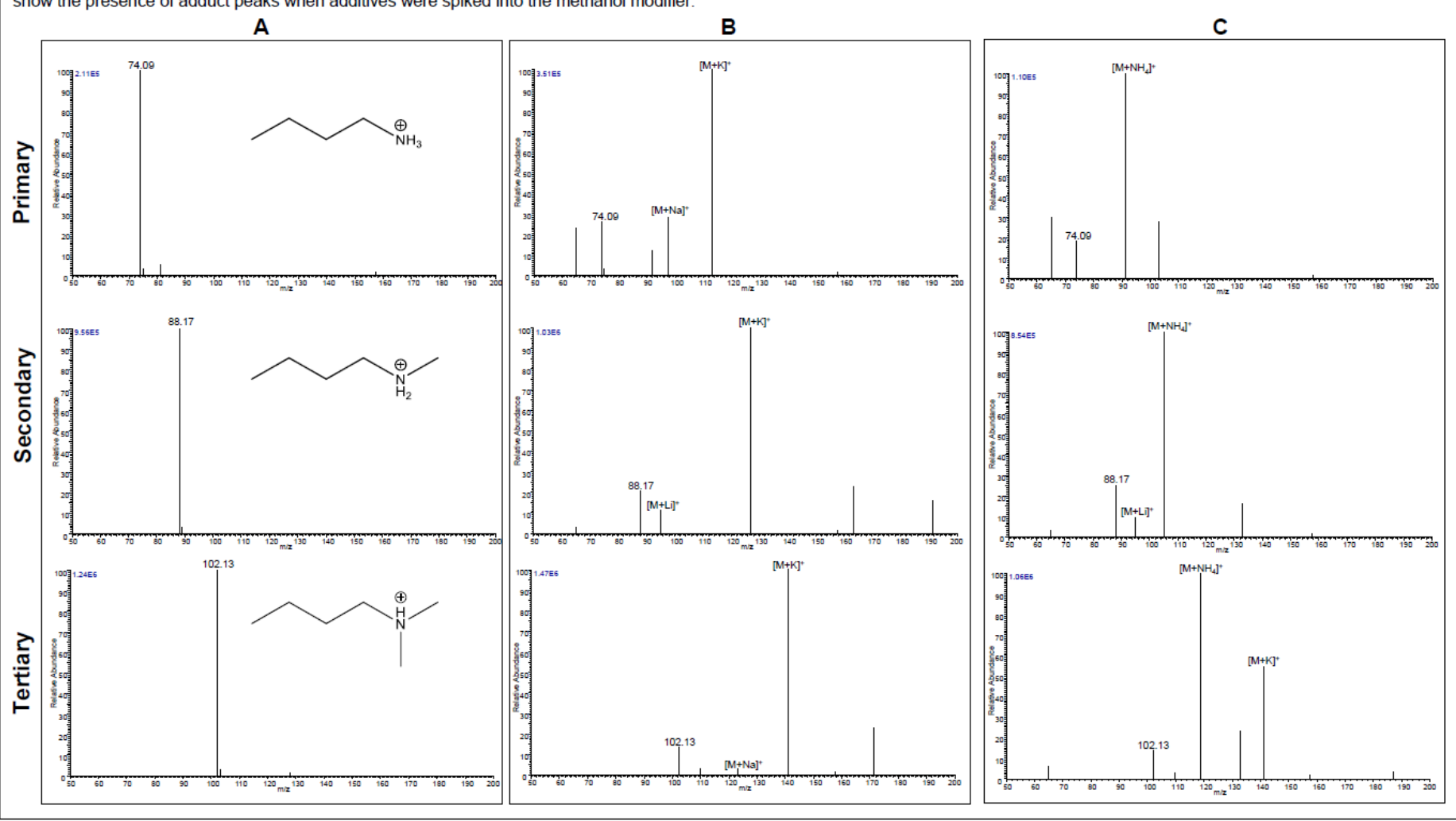
36. Berger, T. A., Effect of density on kinetic performance in supercritical fluid chromatography with methanol modified carbon dioxide. J. Chromatogr. A 2018, 1564, 188-198.

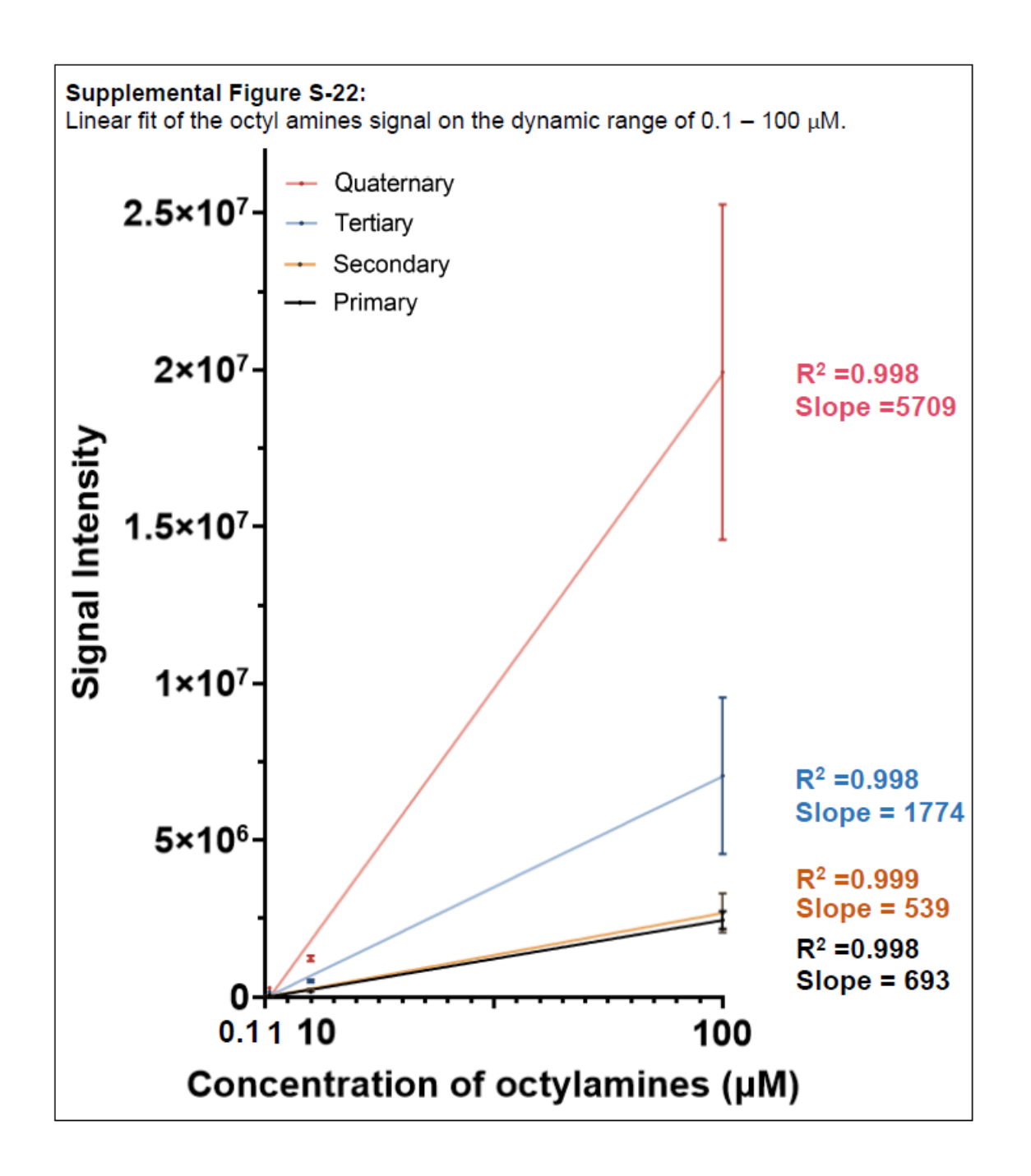
38. West, C.; Melin, J.; Ansouri, H.; Mengue Metogo, M., Unravelling the effects of mobile phase additives in supercritical fluid chromatography. Part I: Polarity and acidity of the mobile phase. J. Chromatogr. A 2017, 1492, 136-143.

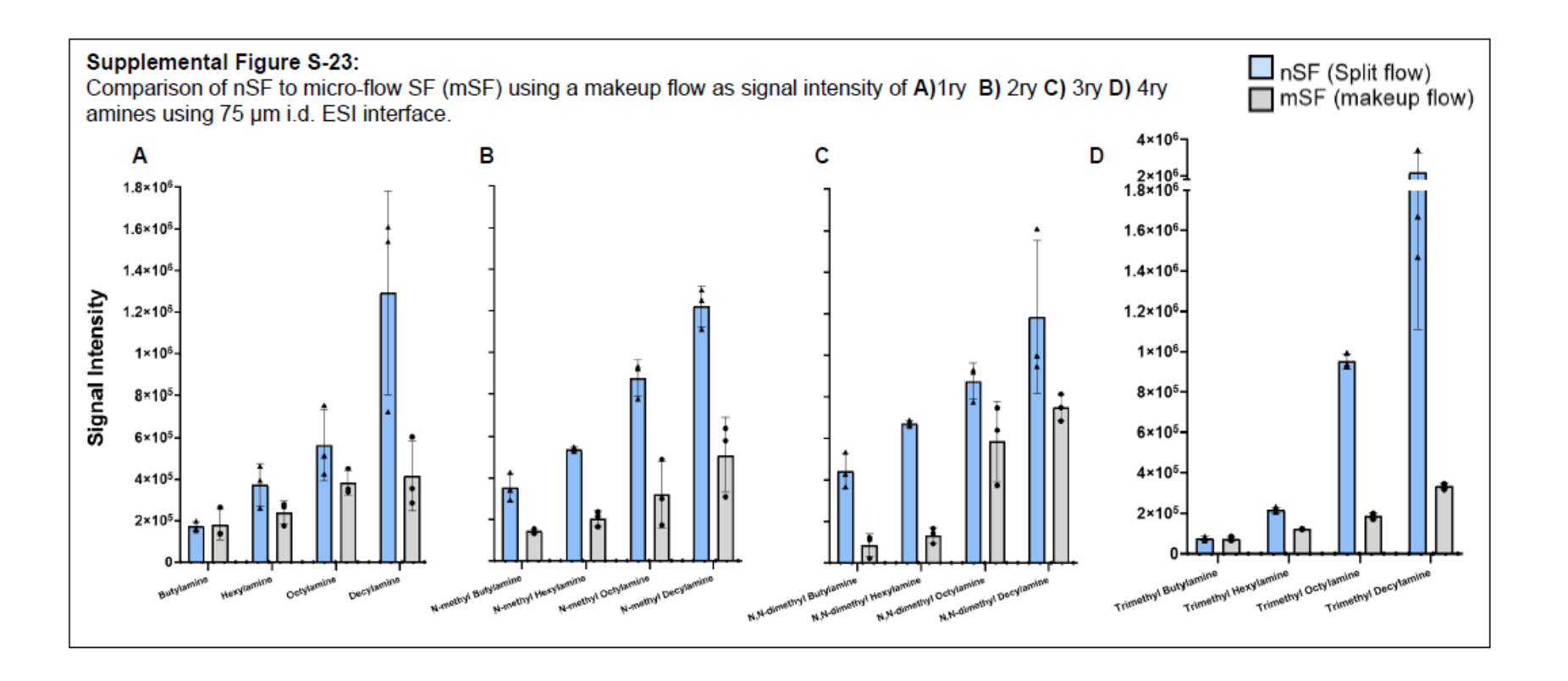
39. Berger, T. A., Characterization of a 2.6µm Kinetex porous shell hydrophilic interaction liquid chromatography column in supercritical fluid chromatography with a comparison to 3µm totally porous silica. J. Chromatogr. A 2011, 1218 (28), 4559-4568.

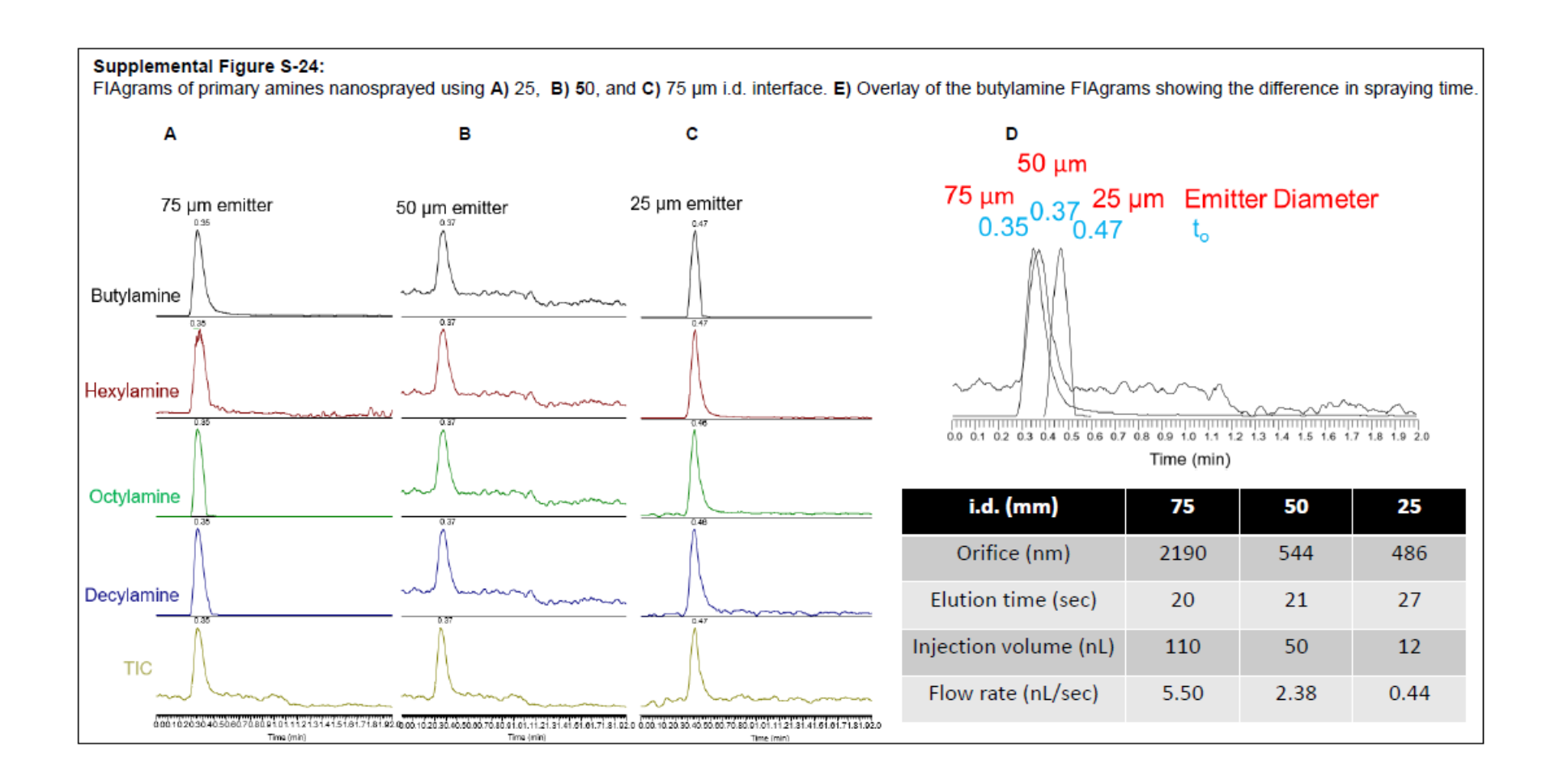


The methanol additives effect on the nSF-MS signal. Nanospraying 1 μL (50μM) of primary (1st raw), secondary (second raw), and tertiary (3rd raw) was done individually with 90% sCO₂ using the 75 μm i.d. capillary interface at 50 °C, 18 MPa. The 10% modifier used was CH₃OH spiked with: A) 0.1% formic acid, B) 1% H₂O, or B) 5 mM ammonium acetate. The MS spectrums show the presence of adduct peaks when additives were spiked into the methanol modifier.

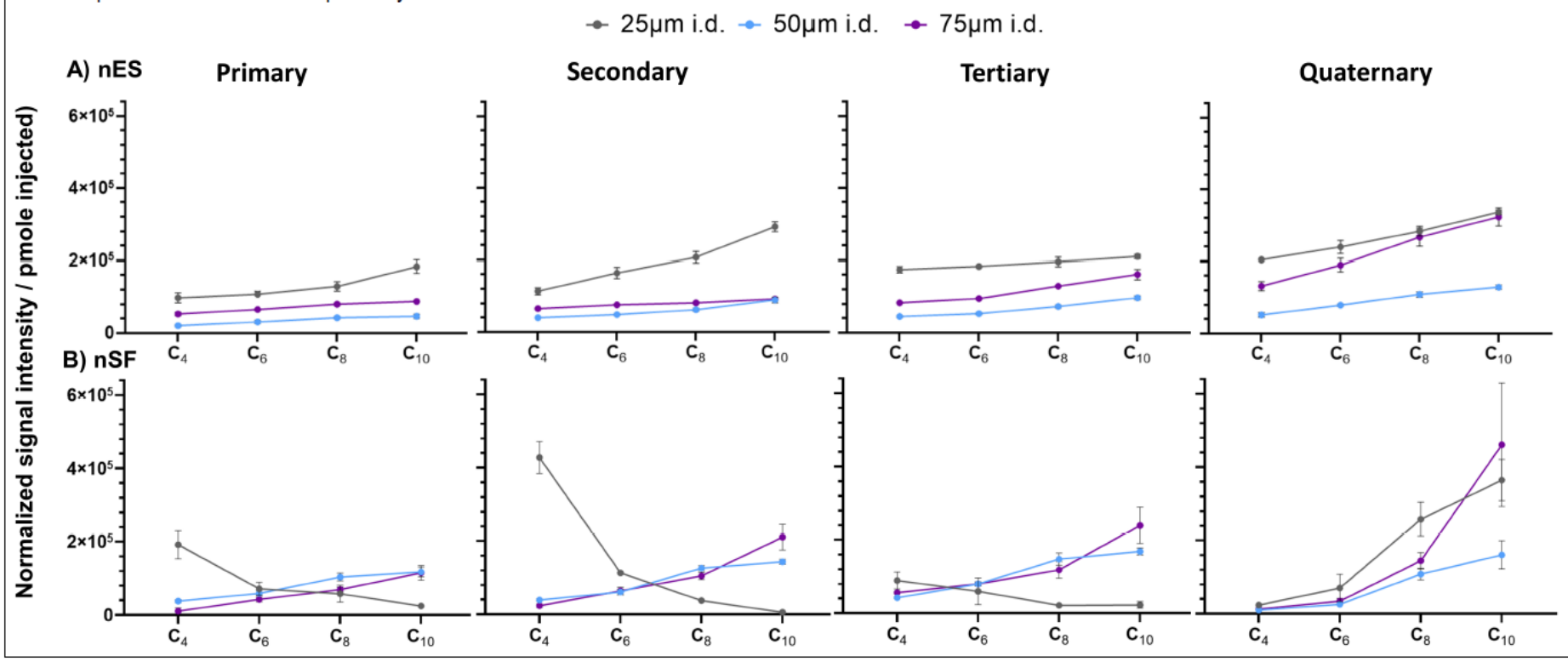


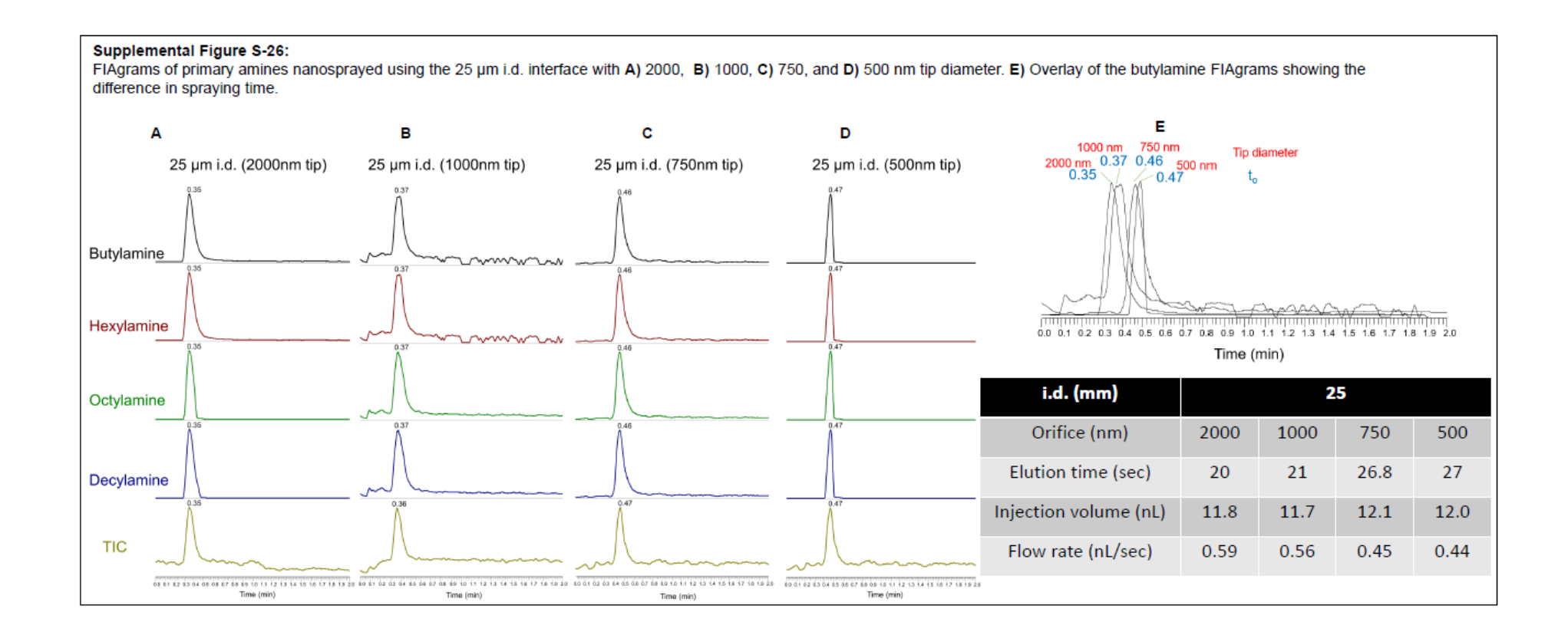


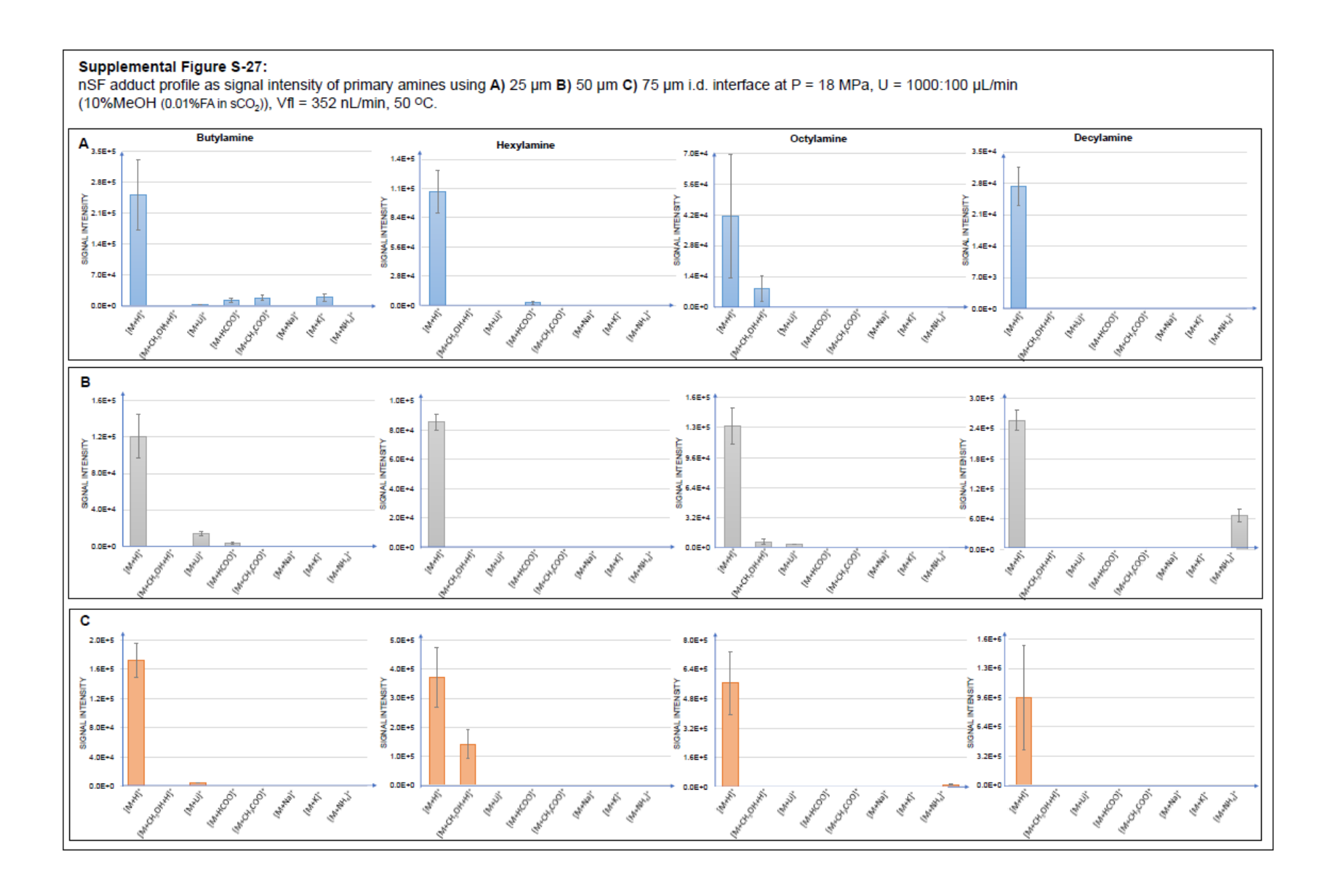


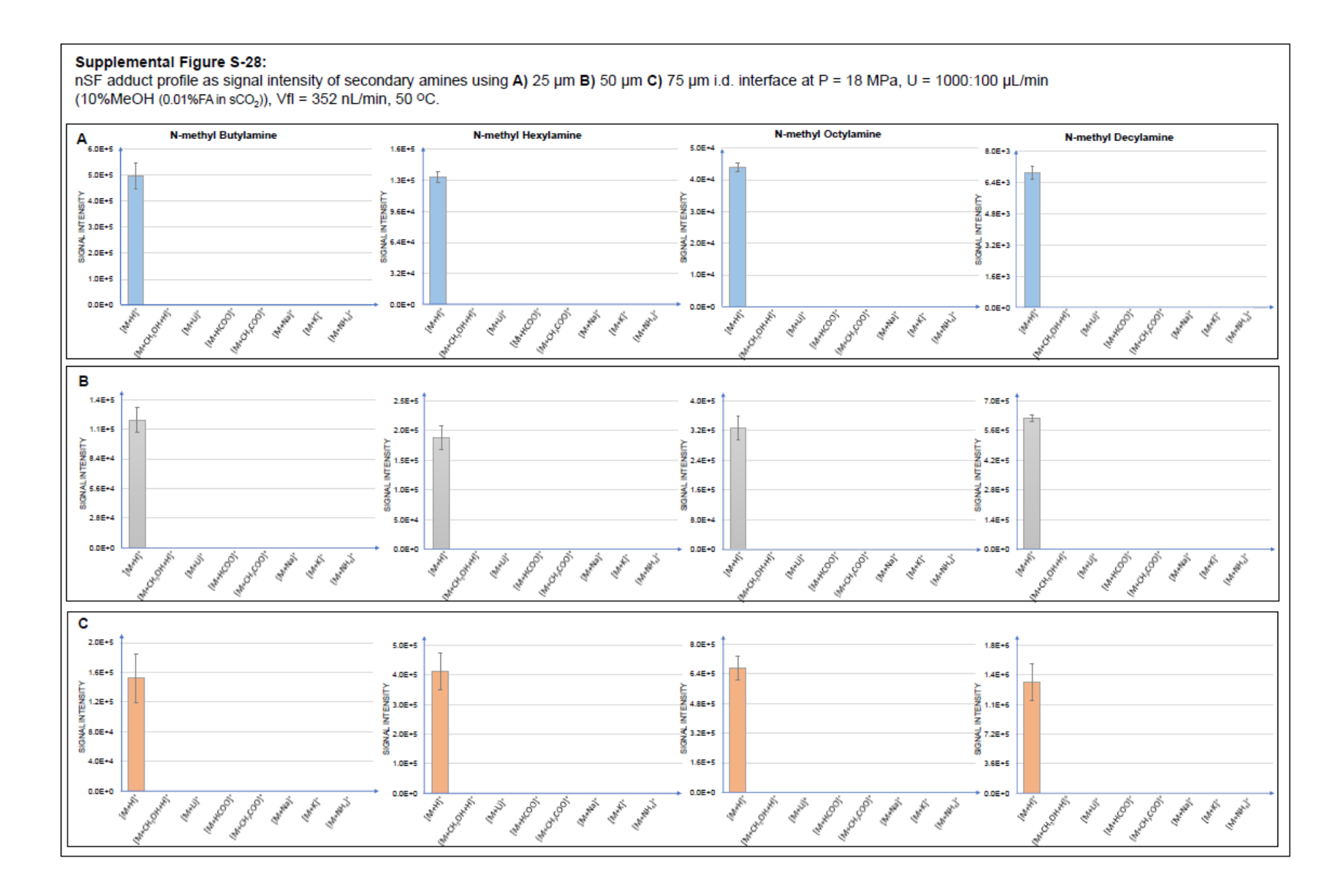


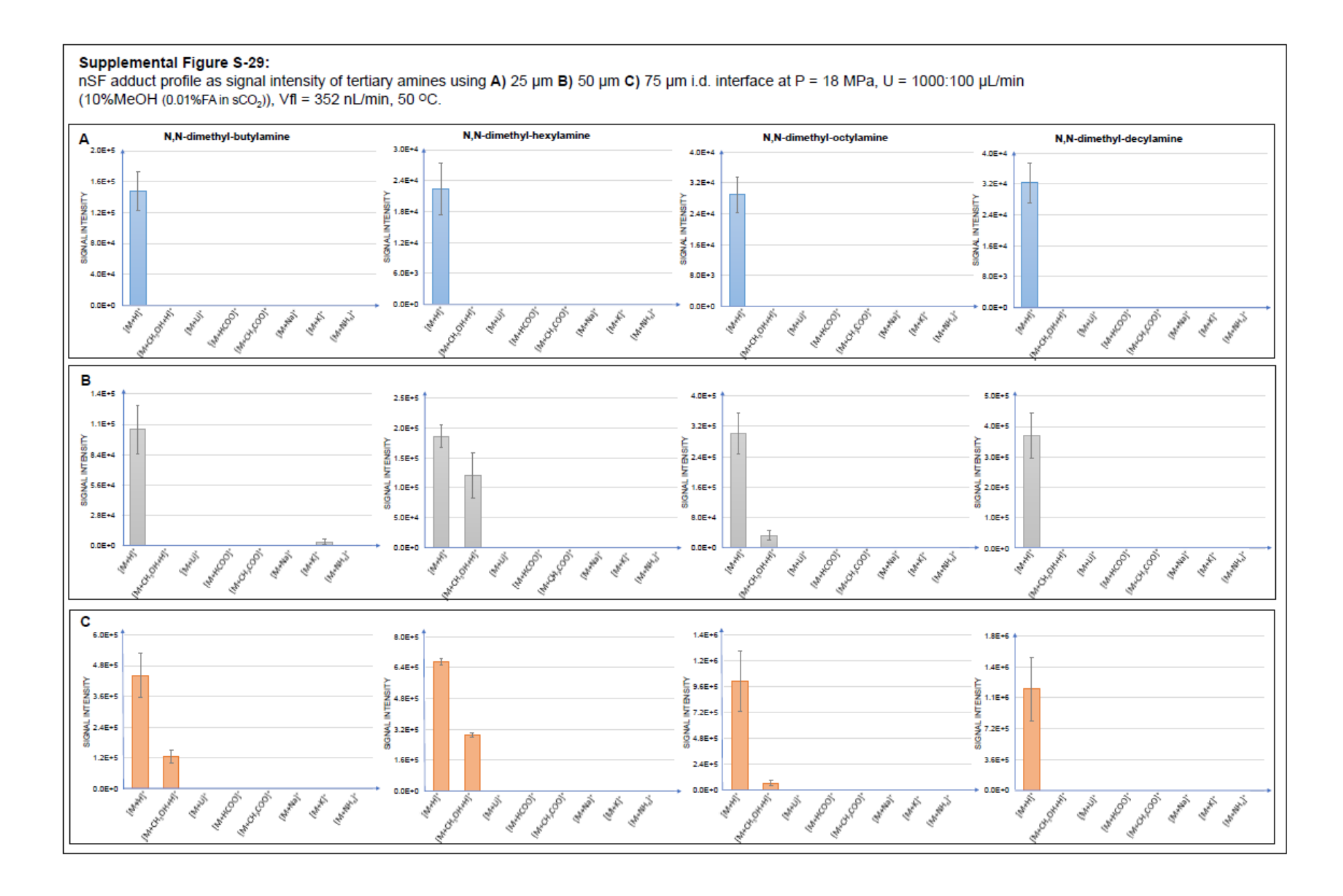
Supplemental Figure S-25: Nanospray ionizing media and emitter tip size effect on MS detection. The MS signal intensity trends of nanospraying 1 μ L of each primary, secondary, tertiary, and quaternary amines individually using A) Organic liquid of 99.9 % methanol and 0.1 % formic acid (nES) and B) Supercritical 90 % sCO2: 10 %methanol (0.1 % formic acid) using 25, 50, and 75 μ m i.d. The signal intensity was normalized to 1.16, 3.16, and 6.40 picomoles injected on the 25, 50, and 75 μ m i.d. nano emitters respectively.

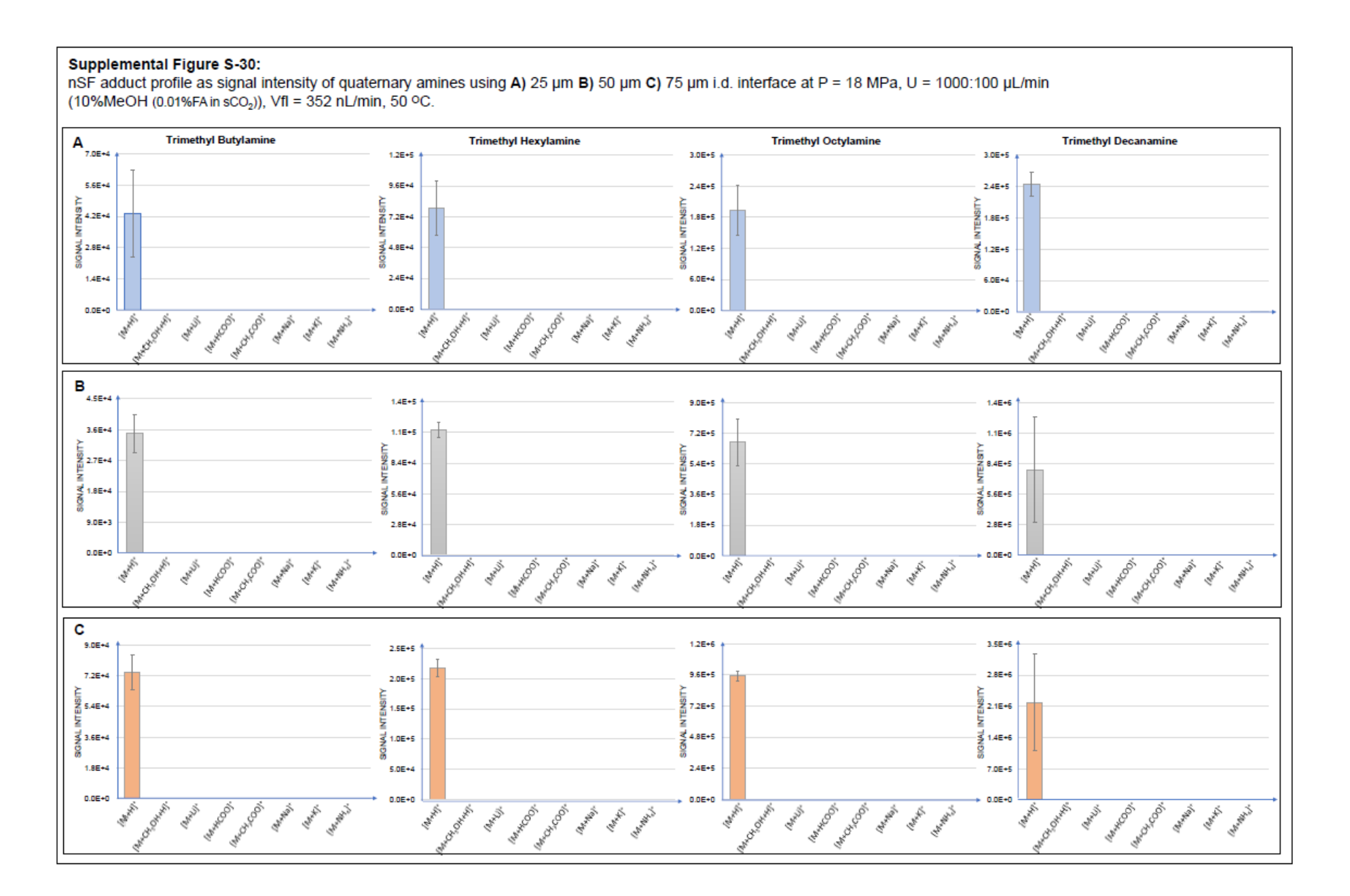












Supplemental Table T-1:

Normalized, experimental, and averages tip diameters of capillary columns laser-pulled, hydrofluoric acid-itched and imaged by scanning electron microscope (SEM).

- A) Normalized laser method (Heat = 42 msec., Velocity = 80 msec., Delay = 150 msec., Pull = 225 msec.).
- B) Edited laser method:
 - 1. For 0.50 µm tip on a 25 µm i.d.: (Heat = 42 msec., Velocity = 50 msec., Delay = 150 msec., Pull = 225 msec.).
 - 2. For 0.75 µm tip on a 25 µm i.d.: (Heat = 580 msec., Velocity = 230 msec., Delay = 235 msec., Pull = 20 msec.).
 - 3. For 1.00 µm tip on a 25 µm i.d.: (Heat = 500 msec., Velocity = 100 msec., Delay = 150 msec., Pull = 200 msec.).
 - 4. For 2.00 µm tip on a 25 µm i.d.: (Heat = 450 msec., Velocity = 50 msec., Delay = 200 msec., Pull = 200 msec.).

Α

	Capillary i.d. (µm)	Normalized tip diameter (µm)	Experime	Average experimental tip diameter (nm)		
	25	0.4	428	549	482	486
	50	0.5	510	438	685	544
	75	2.0	2187	2046	2335	2190
3						

527			
5			
)			
;			

CO2)																							
/min																							
	%CH3OH of Total Flow	5	9	13	17	23	29	33	38	41	44	47	50	52	55	57	58	60	62	63	64	66	67
	%CH3OH of sCO2	5	10	15	20	30	40	50	60	70	80	90	100	110	120	130	140	150	160	170	180	190	20
0	CH3OH flow rate (U) (µL/min)	27.5	55	82.5	110	165	220	275	330	385	440	495	550	605	660	715	770	825	880	935	990	1045	11
	Total nSF flow (mL/min)	577.5	605	632.5	660	715	770	825	880	935	990	1045	1100	1155	1210	1265	1320	1375	1430	1485	1540	1595	16
	nSF Vfl (µL/min) (1/3125split)	0.185	0.194	0.202	0.211	0.229	0.246	0.264	0.282	0.299	0.317	0.334	0.352	0.370	0.387	0.405	0.422	0.440	0.458	0.475	0.493	0.510	0.5
ure	CH3OH pump pressure (psi)	3510	3523	3553	3586	3611	3625	3642	3652	3669	3680	3706	3713				y of solven				ctuation le		
)a)	sCO2 pump pressure (psi)	3480	3496	3506	3525	3531	3542	3549	3561	3611	3640	3652	3660										
	%CH3OH of Total Flow	5	9	13	17	23	29	33	38	41	44	47	50	52	55	57	58	60	62	63	64	66	
	%CH3OH of sCO2	5	10	15	20	30	40	50	60	70	80	90	100	110	120	130	140	150	160	170	180	190	2
0	CH3OH flow rate (U) (µL/min)	32.5	65	97.5	130	195	260	325	390	455	520	585	650	715	780	845	910	975	1040	1105	1170	1235	1
	Total nSF flow (mL/min)	682.5	715	747.5	780	845	910	975	1040	1105	1170	1235	1300	1365	1430	1495	1560	1625	1690	1755	1820	1885	1
	nSF Vfl (μL/min) (1/3125split)	0.218	0.229	0.239	0.250	0.270	0.291	0.312	0.333	0.354	0.374	0.395	0.416	0.437	0.458	0.478	0.499	0.520	0.541	0.562	0.582	0.603	0.
ure	CH3OH pump pressure (psi)	3540	3549	3560	3574	3581	3589	3596	3611	3624	3642	3650	3758	3815	4156	En		of solven	t vapor ex		k sensor a	ctuation le	vel
) (e	sCO2 pump pressure (psi)	3520	3505	3511	3532	3546	3563	3572	3583	3599	3622	3650	3742	3765	4065								_
	%CH3OH of Total Flow	5	9	13	17	23	29	33	38	41	44	47	50	52	55	57	58	60	62	63	64	66	
	%CH3OH of sCO2	5	10	15	20	30	40	50	60	70	80	90	100	110	120	130	140	150	160	170	180	190	2
0	CH3OH flow rate (U) (µL/min)	37.5	75	112.5	150	225	300	375	450	525	600	675	750	825	900	975	1050	1125	1200	1275	1350	1425	1
	Total nSF flow (mL/min)	787.5	825	862.5	900	975	1050	1125	1200	1275	1350	1425	1500	1575	1650	1725	1800	1875	1950	2025	2100	2175	2
	nSF Vfl (µL/min) (1/3125split)	0.252	0.264	0.276	0.288	0.312	0.336	0.360	0.384	0.408	0.432	0.456	0.480	0.504	0.528	0.552	0.576	0.600	0.624	0.648	0.672	0.696	0.
ure a)	CH3OH pump pressure (psi)	3602 3580	3627 3592	3632 3615	3654 3632	3670 3642	3684 3675	3706 3682	3715 3699	3722 3715	3742 3728	3776 3730	3795 3752	3815 3786	3835 3815	3866 3824	4172 4106	Emor	: Density o			ded leak s	
aj	sCO2 pump pressure (psi)										44	47											
	%CH3OH of Total Flow	5	9	13	17	23	29	33	38	41			50	52	55	57	58	60	62	63	64	66	
0	%CH3OH of sCO2	5	10	15	20	30	40	50	60	70	80	90	100	110	120	130	140	150	160	170	180	190	1
	CH3OH flow rate (U) (µL/min) Total nSF flow (mL/min)	42.5 892.5	85 935	127.5 977.5	170 1020	255 1105	340 1190	425 1275	510 1360	595 1445	680 1530	765 1615	850 1700	935 1785	1020 1870	1105 1955	1190 2040	1275 2125	1360 2210	1445 2295	1530 2380	1615 2465	2
	nSF Vfl (µL/min) (1/3125split)	0.286	0.299	0.313	0.326	0.354	0.381	0.408	0.435	0.462	0.490	0.517	0.544	0.571	0.598	0.626	0.653	0.680	0.707	0.734	0.762	0.789	0.
sure	CH3OH pump pressure (psi)	3689	3711	3724	3740	3752	3768	3786	3790	3815	3835	3846	3875	3886	3925	3985	4068	4103	4196	Error: Den	sity of solv		CKO
a)	sCO2 pump pressure (psi)	3621	3654	3686	3706	3720	3742	3734	3756	3787	3816	3833	3845	3865	3911	3956	4000	4086	4131	les	ik sensora		
-,	%CH3OH of Total Flow	5	9	13	17	23	29	33	38	41	44	47	50	52	55	57	58	60	62	63	64	66	
	%CH3OH of sCO2	5	10	15	20	30	40	50	60	70	80	90	100	110	120	130	140	150	160	170	180	190	- 1
0	CH3OH flow rate (U) (µL/min)	47.5	95	142.5	190	285	380	475	570	665	760	855	950	1045	1140	1235	1330	1425	1520	1615	1710	1805	1
	Total nSF flow (mL/min)	997.5	1045	1092.5	1140	1235	1330	1425	1520	1615	1710	1805	1900	1995	2090	2185	2280	2375	2470	2565	2660	2755	2
	nSF Vfl (µL/min) (1/3125split)	0.319	0.334	0.350	0.365	0.395	0.426	0.456	0.486	0.517	0.547	0.578	0.608	0.638	0.669	0.699	0.730	0.760	0.790	0.821	0.851	0.882	0.
ure	CH3OH pump pressure (psi)	3750	3760	3776	3790	3807	3815	3832	3842	3865	3893	3911	3924	3935	3954	4057	4108	4156	4211	4286		sity of sol	_
a)	sCO2 pump pressure (psi)	3632	3680	3712	3732	3756	3786	3811	3821	3833	3850	3890	3905	3915	3924	3985	4065	4108	4142	4251	excer		
	%CH3OH of Total Flow	5	9	13	17	23	29	33	38	41	44	47	50	52	55	57	58	60	62	63	64	66	
	%CH3OH of sCO2	5	10	15	20	30	40	50	60	70	80	90	100	110	120	130	140	150	160	170	180	190	- 1
0	CH3OH flow rate (U) (µL/min)	50	100	150	200	300	400	500	600	700	800	900	1000	1100	1200	1300	1400	1500	1600	1700	1800	1900	2
	Total nSF flow (mL/min)	1050	1100	1150	1200	1300	1400	1500	1600	1700	1800	1900	2000	2100	2200	2300	2400	2500	2600	2700	2800	2900	3
	nSF Vfl (µL/min) (1/3125split)	0.336	0.352	0.368	0.384	0.416	0.448	0.480	0.512	0.544	0.576	0.608	0.640	0.672	0.704	0.736	0.768	0.800	0.832	0.864	0.896	0.928	0.
ure	CH3OH pump pressure (psi)	3790	3807	3810	3822	3837	3842	3850	3862	3876	3892	3918	3935	3956	4086	4122	4186	4233	4265	4315	Error: Den	sity of solv	vent
a)	sCO2 pump pressure (psi)	3680	3695	3742	3762	3784	3798	3816	3825	3842	3865	3906	3931	3954	3986	4065	4123	4135	4272	4295	excer		
	%CH3OH of Total Flow	5	9	13	17	23	29	33	38	41	44	47	50	52	55	57	58	60	62	63	64	66	
	%CH3OH of sCO2	5	10	15	20	30	40	50	60	70	80	90	100	110	120	130	140	150	160	170	180	190	2
0	CH3OH flow rate (U) (µL/min)	62.5	125	187.5	250	375	500	625	750	875	1000	1125	1250	1375	1500	1625	1750	1875	2000	2125	2250	2375	2
	Total nSF flow (mL/min)	1312.5	1375	1437.5	1500	1625	1750	1875	2000	2125	2250	2375	2500	2625	2750	2875	3000	3125	3250	3375	3500	3625	3
	nSF Vfl (µL/min) (1/3125split)	0.420	0.440	0.460	0.480	0.520	0.560	0.600	0.640	0.680	0.720	0.760	0.800	0.840	0.880	0.920	0.960	1.000	1.040	1.080	1.120	1.160	1
ure	CH3OH pump pressure (psi)	3956	3968	3976	3986	3991	4008	4030	4056	4086	4115	4153	4180	4211	4275	4286	4320	4415	4511	4575	4635	Error: Densil	type field and linear
'a)	sCO2 pump pressure (psi)	3758	3790	3826	3886	3942	3954	3968	4007	4022	4068	4120	4152	4195	4201	4235	4295	4376	4495	4520	4611	actual	on leve
	%CH3OH of Total Flow	5	9	13	17	23	29	33	38	41	44	47	50	52	55	57	58	60	62	63	64	66	
	%CH3OH of sCO2	5	10	15	20	30	40	50	60	70	80	90	100	110	120	130	140	150	160	170	180	190	2
00	CH3OH flow rate (U) (µL/min)	75	150	225	300	450	600	750	900	1050	1200	1350	1500	1650	1800	1950	2100	2250	2400	2550	2700	2850	3
	Total nSF flow (mL/min)	1575	1650	1725	1800	1950	2100	2250	2400	2550	2700	2850	3000	3150	3300	3450	3600	3750	3900	4050	4200	4350	4
	nSF Vfl (µL/min) (1/3125split)	0.504	0.528	0.552	0.576	0.624	0.672	0.720	0.768	0.816	0.864	0.912	0.960	1.008	1.056	1.104	1.152	1.200	1.248	1.296	1.344	1.392	1
ure	CH3OH pump pressure (psi)	4115	4118	4125	4138	4150	4165	4186	4215	4221	4248	4265	4323	4418	4525	4612	4680	4782	4862	4943	5108	5206	5
Pa)	sCO2 pump pressure (psi)	3895	4065	4095	4112	4135	4142	4152	4186	4202	4214	4256	4325	4402	4486	4532	4608	4675	4758	4862	5004	5199	52

Supplemental Table T-2: Mobile phase pumps pressure change at 18MPa, 50°C using 75µm i.d. interface as a function of flow rate and %CH3OH different sCO₂ flow rates nSF-MS.

- Mobile phase changed from 5%CH₃OH in sCO₂ until density exceed SF state and instrument stopped at different flow rates.
- Blue highlight are mobile phase pressure (CH₃OH and sCO₂) values.
- Red highlight where percentage methanol gave density error.
- Black highlight where microSF flow rates exceeding nanospray.

Supplemental Table T-3: M06 2X/6 311++G(2d,2p) calculated proton affinities of primary, secondary, and tertiary neutral amines.

Neutral	Proton Affinity/ kJ mol ⁻¹
Butylamine	917.0
Hexylamine	921.5
Octylamine	926.1
Decylamine Decylamine	932.8
N-methyl Butylamine	944.3
N-methyl Hexylamine	948.4
N-methyl Octylamine	957.3
N-methyl Decylamine	955.7
N,N-dimethyl Butylamine	961.8
N,N-dimethyl Hexylamine	965.6
N,N-dimethyl Octylamine	970.3
N,N-dimethyl Decylamine	972.6